A NOVEL ANALOGY: APPLICATION OF HIGHER-ORDER MODE THEORY IN THE MECHANICAL DOMAIN TO THE ELECTROMAGNETIC DOMAIN

A THESIS SUBMITTED TO

THE GRADUATE SCHOOL OF ENGINEERING AND SCIENCE

OF BILKENT UNIVERSITY

IN PARTIAL FULFILLMENT OF THE REQUIREMENTS FOR

THE DEGREE OF

MASTER OF SCIENCE

IN

MECHANICAL ENGINEERING

By

Mehmet Kelleci

August 2018

A NOVEL ANALOGY: APPLICATION OF HIGHER-ORDER MODE THEORY IN THE MECHANICAL DOMAIN TO THE ELECTROMAGNETIC DOMAIN

By Mehmet Kelleci

August 2018

We certify that we have read this thesis and that in our opinion it is fully adequate, in scope and in quality, as a thesis for the degree of Master of Science.

Mehmet Selim Hanay(Advisor)

Burhanettin Erdem Alaca

Talip Serkan Kasırga

Approved for the Graduate School of Engineering and Science:

Ezhan Karaşan
Director of the Graduate School

ABSTRACT

A NOVEL ANALOGY: APPLICATION OF HIGHER-ORDER MODE THEORY IN THE MECHANICAL DOMAIN TO THE ELECTROMAGNETIC DOMAIN

Mehmet Kelleci
M.S. in Mechanical Engineering
Advisor: Mehmet Selim Hanay
August 2018

It is crucial to engineer novel detection schemes that can extract information pertinent to the morphological properties of the analytes for widespread usage of lab-on-a-chip technology. Within the scope of this thesis, a novel method that is originated in mechanical domain based on NEMS resonators is adapted to electromagnetic domain with employment of electromagnetic resonators operate in microwave regime. The viability of the proposed method is assessed both by experiments and simulations. The designed microfluidic channel embedded microstrip resonator is driven at its first two resonant modes simultaneously by a phase-locked loop to detect the analyte passage events within the channel. The attained resolution is $2\text{x}10^{-8}$ for both modes at the response time in terms of allan deviation. With the detection scheme we constructed, the location and electrical volume of the microdroplets and cells are obtained. It is shown that the two-mode detection scheme based on microwave resonators can be extended to applications that exploits even higher-order modes to obtain the size, orientation, skewness and permittivity information of the target analytes. Morevover, the framework presented here forms a base for a novel imaging application that can be alternative to optical microscopy.

Keywords: microwave resonators, cell detection, resonant mode, microwave imaging.

ÖZET

YENİ BİR ÖRNEKSEME: MEKANİK ALANINDAKİ ÇOKLU MODLAR TEORİSİNİN ELEKTROMANYETİK ALANINDA UYGULANMASI

Mehmet Kelleci
Makine Mühendisliği, Yüksek Lisans
Tez Danışmanı: Mehmet Selim Hanay
Ağustos 2018

Çip üstü labaratuvar teknolojisinin gelişmesi ve yaygınlaşmasına adına hücre, organel gibi biyolojik numunelerin morfolojik özelliklerini elde edebilecek yeni yöntemler geliştirmek önem taşımaktadır. Bu bağlamda, mekanik alanındaki nanoelektromekanik sistem temelli yüksek modlar uygulamasının, elektromanyetik alanında mikrodalga rezonatör temelli bir karşılığı geliştirildi. Geliştirilen uygulamanın hem simulasyon ortamındaki hem de deneysel olarak başarısı test edildi. Dizayn ettiğimiz mikroakışkan kanal gömülü mikrostrip rezonatörü ilk iki rezonans modunda sürebilecek ve hücre, damlacık gibi analitlerin kanaldan geçişlerini algılayabilecek bir faza kilitli döngü tasarlandı. Elde edilen çözünürlük iki mod için de Allan sapması bazında $2\text{x}10^{-8}$ olarak hesaplandı. Oluşturulan algılama sistemiyle kanaldan geçen damlacıkların ve hücrelerin pozisyonları ve elektriksel hacimleri, frekans kaymalarından başarılı bir şekilde hesaplandı. Dizayn ettiğimiz ilk iki rezonans moduna bağlı algılayıcı, bu metodun daha yüksek modların da kullanılarak hedef biyolojik numunelerin ebat, oryantasyon, eğrilik ve permitivite gibi morfolojik ve elektriksel özelliklerinin elde edilebileceğini kanıtlar niteliktedir. Bununla birlikte, sunduğumuz uygulama optik mikroskopiye bir alternatif oluşturabilecek, mikrodalga rejiminde çalışan bir görüntüleme uygulamasının temelini oluşturmaktadır.

Anahtar sözcükler: mikrodalga rezonatör, hücre algılama, rezonans mod, damlacık algılama, mikrodalga görüntüleme.

Acknowledgement

I acknowledge my thesis advisor Prof. Dr. Mehmet Selim Hanay for his constant support and interest in my studies and academic career for the past five years. His pinpoint advises and scientific approach to the problems we faced during our researches taught me a lot and expedited the processes. Our meetings in the laboratory and conference halls were always joyful and enlightening. Besides technical aspects, I learned about patience, management and how to think the potential future impact of a project from him. His multidisciplinary background and extensive research experience is an inspiration for me and to many other students. Being the archetype of an excellent academician with a gentle soul, I will always remember him with admiration and utmost respect.

I would like to thank Hande Aydogmus, without her efforts this work would be only a compressed version of this. We never had a conflict of interest in our studies, planned our careers together and took care of each other. I would like to thank Eren Özgün who has to endure similar challenges in life as I do, we always had a close frequency and understood each other. I kindly thank Selçuk Oğuz Erbil with whom I attended countless events, projects and demonstrations. We had plethora of amusing and absurd memories together. I sincerely thank Mumun Yildiz for his unconditional help and presence. We share an almost same background with all our boarding student past; we are the ones that can enjoy the silence and survival.

I thank all the rest of my friends from the KAL dormitory to the Bilmech for their company and surprise birthday parties. Since my departure from my hometown I never had lack of friends which I consider as a great luck. They are truly intelligent and funny people. For me each one of them is a unique wavelength in the social spectrum that made Ankara steppes colorful for me.

Finally, I sincerely would like to thank my dear parents Nizamettin and Gülten and my elder brother Ceyhun for their labour, love and support for me.

Contents

List of Figures

Chapter 1

Introduction

1.1 The Resonance Phenomenon

The resonance phenomena have different yet similar explanations in many domains such as mechanical, electrical, electromagnetic, and optical. In mechanical domain, the resonance is defined as a system's oscillation at greater amplitudes at specific frequencies. For the mechanical systems, the resonance occurs when the frequency of the driving force matches the natural frequency of the system. The natural frequency of the system is defined as $w_n = \sqrt{\frac{k}{m}}$ where m is the mass and k is the spring constant.

For instance in mechanical domain nanoelectromechanical systems(NEMS) can be given as good examples where the resonance phenomenon is widely exploited. NEMS are the product of the pursuit of ultrahigh sensitivity for biotechnology, measurement of minute forces and displacements hence sensor technology, next generation computer technologies and so on [1]. NEMS structures have resonant frequencies at microwaves, very high quality factors on the orders of tens of thousands, effective masses around femtograms, at least one size parameter is on the order of nanometers and many other unprecedented properties[2]. The most popular configurations in NEMS are doubly clamped beams and cantilever

beams which are ubiquitous in atomic force microscopy (AFM) applications. One intriguing aspect of these structures is that the continuum approach is still valid even at that size so that the modelling can be accomplished by solving the euler-bernoulli beam equation. There are three main sub operation schemes exist in the whole system. First stage is the input transducer which is necessary to drive resonator at its resonant frequency, converts the electrical signal into mechanical displacements to excite the structre. Another is named as the control signals which stands for the external perturbations to the system that can modify the resonant frequency and quality factor of the structure. The outermost is called output transducer that converts the mechanical displacement into electrical signals so that the information carrying signals can be obtained for observation. The fundamental operation scheme of NEMS for particle sensing is the modulation of the effective mass. The excitation transducers can be based on magnetomotive, thermal or piezoelectric methods. Similarly the output transducer can rely on magnetomotive, piezoelectric and optical methods.

Pertaining to this thesis NEMS structures can be employed for detection of particles such as nanoparticles, protein molecules and cells. For instance, doubly clamped beam configurations are frequently employed for particle sensing applications. The fundamental operation scheme in these structures is that they are manufactured with advanced nanomanufacturing methods -such as depotision, soft lithography, dry and wet etching, molecular beam epitaxy, atomic layer deposition- and the top surface is covered with a specific layer of polymer that would allow only specific particles to adhere on them. Then in a controlled and isolated environment the target particles are sent onto the structures. If a particle is adhered on the surface of the structure then the effective mass of the whole structure changes due and related to the presence of the particle on the surface. Consequently the resonant freqeuncy of the structures changes since the term m is modified in the formula. The frequency shift of the system depends on the size and weight of the adhered particle. As mentioned previously the layered polymer is permeable to only the predetermined target particles. Since at that scale each particle has unique size and weight they create specific frequency shifts. Hence it is possible to use this information to characterize the particles adhered

on the structure. As a remarkable example, this operation scheme can find itself an application area in cancer detection. A significant example is [3], where for the first time the detection of a biomolecule is realized. Since each particle have unique nominal masses as mentioned previously, they cause unique nominal frequency shifts that allow the experimentalist to characterize the adhered particle. The experiments with the structure in [3] was successful to characterize the gold nanoparticles of mean radius 2.5 nm by frequency shifts data.

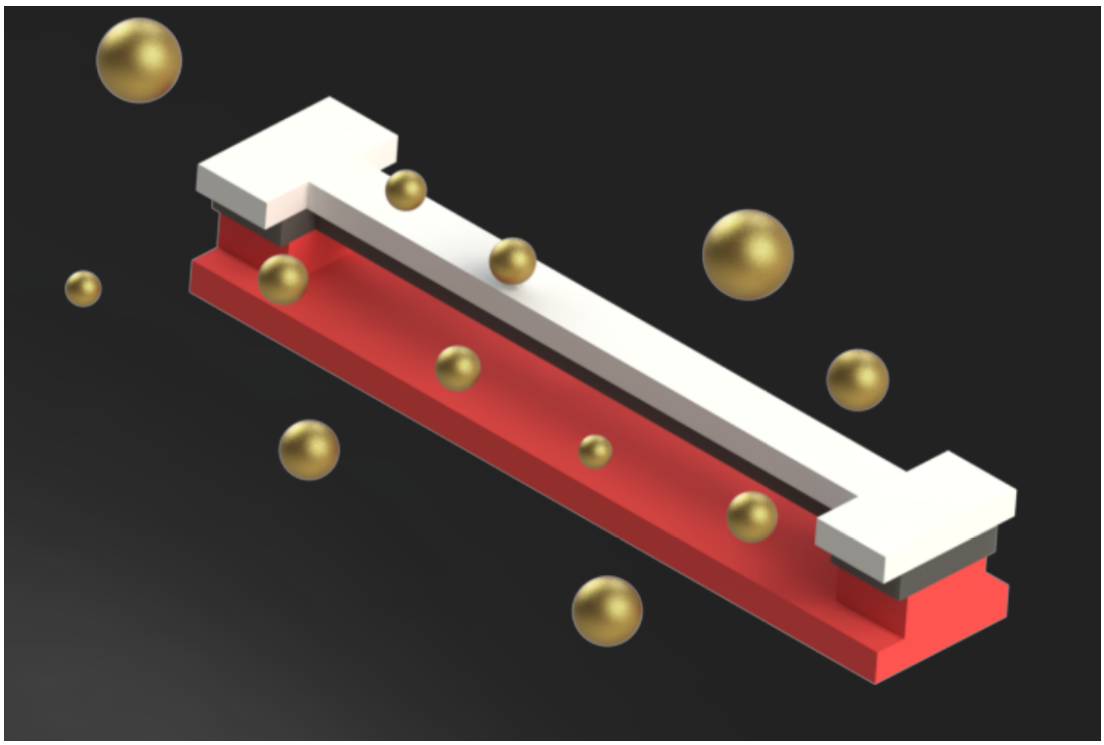

Figure 1.1: Depiction of particle adhesion on doubly clamped NEMS

It is shown that a mass sensitivity approximately of $2x10^{-18}g$ can be ascertained by these structures in previous studies[4]. During efforts spent on NEMS the reported values keep getting closer to the theoretical limits. In carbon-nanotube based cantilever structures the atomic resolution limits are shown to be reached $1.3x10^{-25}kgHz^{-1}$ [5] by realizing the detection of gold atoms.

Certain biological applications require aqueous environments for living samples to sustain their vitality. The quality factors of clamped beams and cantilevers

drop exponentially when they are drenched. A novel solution was proposed to the problem by Manalis group. In their structures the cantilever structures contain embedded microfluidic channels with continuous flow allow cells move along the entirety of the channel [6]. Since the cells are in their natural environment they can maintain their life cycle and it is possible to observe the changes in their masses as they flow with the carried fluid. Besides since the cantilever is planted in aerial environment quality factor decrement is not an issue.

NEMS research field is quite vivid and attracts attention in various ways such as increasing the quality factors of the structures, improving the excitation and read out schemes and adaptation of the structures for mass production.

In the electrical domain the resonance occurs when the impedance of the circuit is purely real happens when the admittance and susceptance values cancel out each other, consequently according to the series or parallel configuration the impedance tend to go zero or infinity. The extremities in impedance at resonance makes the RLC circuits good candidates for designing band-stop filters. If the resonant circuit is composed of nondissipating elements which are inductor and capacitor a very high quality factor can be reached. In these circuits very high voltages and currents can be generated so that they can be explotided voltage/current magnifiers. A good example to these circuits are LC tanks. At resonance the circuit stores energy and that energy vascillates between the capacitor and inductor until all the energy dissipates.

In the eletromagnetic and optical domain, the resonance phenomenon occurs when the incident and reflected waves form standing wave patterns so that the structure can store energy. The resonators can be built in microwave regime by confining the electromagnetic waves in a conductive closed container so that the travelling electromagnetic fields can form standing wave patterns; these type of structures are called microwave cavity. Another form can be constructed by using open or short ended transmission lines. In that type of transmission lines due to the abrupt changes in impedances at the boundary conditions incident and reflected waves bounce back and forth to create specific patterns of electrical field; which are called standing wave patterns so that the structure can store energy.

These structures can be used to built high frequency filters, impedance matching circuits or antennas. Pertaining to this theses the writer will be interested in the sensor applications based on these structures.

For sensory applications in NEMS, it mentioned previously that the main modulation parameter was the effective mass. When it comes to the electromagnetic domain the fundamental modulation parameter is the effective permittivity -also called as dielectric constant- of the structure. An electromagnetic structure begin to resonate at certain frequencies according to its geometrical and electrical characteristics and their reflection in Maxwell's equation. One decisive electrical parameter in these equations that tells us at what frequency resonance occur is effective permittivity. Permittivity is defined as a material's resistance against forming electrical field within. For all the materials permittivity values are defined based on the permittivity of free space ($\epsilon_o = 1$) hence in the literature permittivity values of materials are called relative permittivity ϵ_r. For each material this value is dependent on frequency, temperature and polarization effects.

Almost all of the resonating microwave structures can be employed as sensors by tailoring them according to the purpose. Microwave cavities, microstrip transmission lines, coplanar waveguides and microstrip ring resonators are all good candidates for sensor applications. The extraction of information is based on frequency shifts most of the time yet amplitudes of the transmission coefficients (s parameters) can also be used.

Permittivity is defined as a material property. However, when there are multiple layers of materials in a structure, according to their geometry and positioning an effective permittivity definition comes into play. For instance when a microwave transmission line is considered, there is a dielectric filling materials sandwiched between an upper and lower conductor. Besides, the whole structure is surrounded by air which has its own permittivity; therefore an effective permittivity that stands for the whole structure is needed. And the most intriguing aspect of this issue is that any volume of imperfection within the dielectric filling material reflects its presence on resonant frequency of the structure. The idea to use these structures for particle sensing stems from this fact.

For instance in the work [7], a microstrip ring resonator is used as a humidity sensor. The resonant frequency of the structure is given as $f_c = \frac{c}{L_{ch}\sqrt{\epsilon_{eff}}}$ and the resonator is placed in an empty enclosed environment. At the initial state the device resonates at a specific frequency according to the environment characteristics. However when the experimentalist sends the air with different humidity levels resonance frequency shifts since the effective permittivity is modulated by the humid air. By sending air with varying humidity levels, purging the control volume with a clean gas such as N_2 after sending air and noting down the frequency shift caused by the level of humidity, it is possible to characterize the humidity level. A very similar work [8] accomplishes the same goal with a transmission line (TL) resonator. The TL resonator is placed in a control volume and materials with foreknown permittivities are sent to the control volume. Once the control volume is filled with the material, a measurement of S_{21} parameter with a vector network analyzer (VNA) is taken. It is observed that as the permittivity increases the resonant frequency drops accordingly.

A resonating waveguide structure is called a microwave cavity. In these structures the electromagnetic waves are sent through a free space which is enclosed by conductive surfaces. At the resonance situation the incident and reflecting waves form specific patterns and transmission parameters reach extreme values. For instance in a waveguide at resonance the forward transmission coefficient S_{21} reaches its maximum. A waveguide as a sensor application is accomplished in [9]. In the structure a channel for liquid flow is embedded. Experiments are realized with several liquids with varying concentration. At each time the resonance frequency and the magnitude of S_{21} is recorded. Latter these values are used to characterize the liquids and map the concentration level of liquids. A non-destructive and novel approach microwave analysis is developed in [10] where the resonant structure is a cylindrical cavity. Since at the microwave frequencies the electromagnetic waves can easily penetrate through low loss materials it is possible to extract information about the type of the material, size, particle distribution and contamination. In the study the sample to be studies is placed in the middle of the closed cylindrical cavity. From one port the excitation is realized and from the other port where waves interacted with the sample placed goes out

to the VNA. According to the placed polymers S_{11} and S_{21} are measurements are taken. The best responsivity with respect to frequency for different types of polymers are located. The frequency shifts with respect to sample type are promising for developing a novel low cost and rapid polymer characterization method based on microwave analysis with cavities. The material characterization methods with microwave cavities open new ways for early diagnosis in medical applications. For instance, lactate detection in cerebrospinal fluid is crucial for a patient's future healt. A cylindrical cavity excited by a patch antenna is used [11] to monitor the lactate levels in water. As mentioned previously the other microwave resonant structures that can be employed in sensing are microstrip transmission line resonators, ring resonators and coplanar waveguide [12] resonators. Likewise in the study where the lactate levels are measured with cavities are accomplished by an LC-tank resonator coupled to a microstrip line [13]. According to the concentration of the water flow the resonant characteristics of the structure is modified so that the glucose level within the flow can be quantified.

Microwave sensing techniques are non-contact methods that exploits the penetration of electromagnetic waves into the materials to be measured. By increasing the quality factor of resonators with active circuitry [14] it is possible to obtain high resolution resonators with large penetration distances.

A popular and vivid research branch in microwave sensing applications is microwave resonators embbedded with microfluidic channels. This configuration of sensing promises on table products for realizing bio-analyses, medical tests, label-free cell characterization, detection of target cancer cells in biological samples for early diagnosis, cell counting and quantification and many more aspects for next generation lab-on-a-chip applications with wide applicability and low cost. In the previous works given as literature research the measurements are taken after the sample is planted within the sensing region. Microfluidic implementation allows the experimentalist to take measurements continuously and analyse the sample in a short time related to the flow rate. All the mentioned structures from cavities to ring resonators are available for microfluidic application except embedding a channel within the sensor is a little more demanding manufacturing process. Similarly, dielectric measurements [15], [16] and environmental effects

on dielectric properties [17] for liquid flows can be accomplished with microfluidic embedded microwave resonators. Yet, they host a conspicuous and practical use for biological applications which is cell counting and characterization. Most of the microwave sensors developed upto this date focused on material and flow properties as whole. However recent researches shows that the resolutions of these sensor are capable of sensing nano particles and biopolymers [18]. By means of incorporating capacitive changes with coupling a microwave TL resonator to an interferometer it is shown that a detection limit of 650zF -which is enough to measure the presence of living cells at that configuration- at 1.5 GHz operating regime is reached [19]. On a greater sensing scale yet for a very large throughput, a microwave sensor for droplet counting and concentration characterization is developed. This system is capable of counting droplets generated at a throughput of 3.33 kHz such as fetal bovine serum, penicilin antibiotic mixture, milk and glucose [20].

Until this point the writer of the thesis made effort to draw attention to the similarities between the NEMS based sensors and microwave resonator based sensor applications. In NEMS the fundamental modulation parameter is effective mass whereas this parameter becomes effective permittivity when it comes to the microwave sensing applications. Sensing and frequency shifts occurs in case of particle adherence on surface of NEMS whereas frequency shifts come into play in case of any presence of particle in the vicinity of electrical field of microwave resonators. For the read out of the information carrying signals these two vivid research branches merges as novel sensor applications [21]. Moreover, the theory behind these sensor applications can also overlap for higher order mode sensor applications. This aspect is the core of this thesis which establishes an unprecedented analogy between mechanical and electromagnetic domain.

1.2 A Novel Analogy

The foundations of the analogy we established between the mechanical and electromagnetic domains derives from NEMS in the first domain. Previous studies

in NEMS have shown that the employment of higher modes [22], [23] enables the current state-of-the-art devices can be used to determine the position, mass, size and asymmetry of the adsorbed molecules. By continuously recording the frequency shifts caused by discrete molecule adsorption events and combining it with the mode shapes of the structure in the higher order mode theory it is possible to reach the information about the particles stated above. For the first time this paradigm is realized by merely using the first two modes with a statistical approach[22]. Later on it is widened for higher orders modes to pursue more information about the particles[23]. In this section it will be explained that this theory can be extended to electromagnetic domain.

1.2.1 Higher-Order Mode Theory in Mechanical Domain

At this stage to form a basis for explanation of the electromagnetic counterpart of this NEMS resonator application the writer of the thesis elaborates the higher order mode theory mathematically in mechanical domain.

In the case of a particle adsorption on the surface of the device the maximum kinetic energy of the device do not chance since the mode shapes are assumed to be invariant and particles are much smaller than the device itself. There fore the kinetic energy of the excited device before and after the particle adsorption [23] are stated as follows.

$$KE_{unloaded} = \frac{1}{2}(w_n^o)^2 \int_{\Omega} \rho_{dev} |\Phi_n|^2 dV \tag{1.1}$$

$$KE_{loaded} = \frac{1}{2}(w_n)^2 \int_{\Omega+\Omega_{an}} (\rho_{dev} + \rho_{an}) |\Phi_n|^2 dV \tag{1.2}$$

Where the Φ is the unchanged mode shape, Ω and Ω_{an} are the spatial integration domain of the device and the analyte respectively, ω_n^o and ω_n are the angular resonant frequencies of the unloaded and loaded device respectively and ρ_{dev} and ρ_{an} are the mass density of the device and the analyte respectively.

The surface loading due to presence of an analyte on the surface is expressed as below. The integration is performed on the spatial integration domain of the analyte since the adsorption events are regarded as discrete hence no other loading occurs on the surface by an external agent.

Volume integral for the analyte can be replaced by the following expression.

$$\int_{\Omega_{analyte}} \rho|\Phi_n|^2 dr = \int_{\Omega_s} \mu(r)|\Phi_n|^2 dS$$

After equating equations 1 and 2 and a-manipulations the following form can be achieved.

$$\frac{w_n^{o2} - w_n^2}{w_n^2} = -\frac{\int_{\Omega_s} \mu(r)|\Phi_n|^2 dS}{\int_{\Omega} \rho_{dev}|\Phi_n|^2 dV} \tag{1.3}$$

Now, it is important to emphasize the fact that the frequency shifts are minute compared to the fundamental resonant modes. The terms $w_n^o \approx w_n$ therefore $w_n^o + w_n = 2w_n^o$ and $w_n^o - w_n = \triangle w$. Henceforth equation 3 can be rearranged as:

$$\triangle_n \approx \frac{w_n^o - w_n}{w_n} = \frac{-1}{2}\frac{\int_{\Omega_s} \mu(r)|\Phi_n|^2 dS}{\int_{\Omega} \rho_{dev}|\Phi_n|^2 dV} \tag{1.4}$$

Each mode shape Φ_n are normalized by assumption that the device has constant density along its entirety with respect to the condition:

$$\int_{\Omega} \rho_{dev}|\Phi_n|^2 dV = M \tag{1.5}$$

Also note that the mode shapes are pure sinusoids due to stagnant boundary conditions of the doubly clamped beam that satisfies the orthonormality via the integral of the sinusoids over a period:

$$\int_{\Omega} \Phi_n . \Phi_n dV = 1$$

The surface loading on the device engendered by the presence of analytes are defined as follows:

$$F_n = \int_{\Omega_s} \mu(r) |\Phi_n|^2 dS$$

Therefore after necessary manipulations the F_n term can be related to the experimentally obtained frequency shifts as follows:

$$F_n = -2M \triangle_n \tag{1.6}$$

At this stage the conspicuous aspect of the multi-mode sensing theory emerges. It will be shown in a while that the moments of the linear mass distribution $\mu(r)$ function can be exploited to reach the mass, position, size and extent of the analyte. Initially, $\mu(r)$ term is unknown yet can be reached and linked to the experimentally obtained frequency shifts via moments of the function. The link between the frequency shift and moments of the function stems from the paradigm that the functions $g^k(r)$ can be approximated as linear combinations of mode shapes as follows.

$$g(r)^k = \Sigma_{n=1}^{N} \alpha_n^k |\Phi_n|^2 \tag{1.7}$$

Consequently by leaving the mass distribution term $\mu(r)$ unknown, making deductions about the terms related to it by merely manipulating the frequency shifts occurred in the resonant modes with the weighting coefficients as follows:

$$m^k = \int_{\Omega_s} \mu(r) g^k(r) dS = \Sigma_n^N \alpha_n^k \int_{\Omega_s} \mu(r) |\Phi_n|^2 dS = \Sigma_n^N \alpha_n^k F_n \tag{1.8}$$

Finally restating the equation 1.8 to clearly express the fact that the moments of $\mu(r)$ can be reached through the frequency shift, mass of the device and calculated weighting coefficients is important:

$$m^k = -2M\Sigma_{n=1}^{N}\alpha_n^k \triangle_n \tag{1.9}$$

But how does the moments aid to reach information in practice? The kth order g(r) function is defined as $g(r)k = r^k$ therefore $g(r)^0 = 1$, $g(r)^1 = r$ and $g(r)^2 = r^2$ and so on. When the zeroth moment of the areal mass density $\mu(r)$ function is taken $\int_{\Omega_s} g^0(r)\mu(r)dS = m = m^0$, the mass of the analyte is reached as it can be seen in the equation. For obtaining of higher order moments please see the appendix.

1.2.1.1 Determining the Weighting Coefficients

Now, how the weighting coefficients are determined. The answer comes from the least squares method. Define the function e as follows:

$$e(\alpha_i^k) = \int (\Sigma_{n=1}^{N}\alpha_n^k|\Phi_n|^2 - g_{exact}(x))^2 dx \tag{1.10}$$

The condition coefficients are determined according to the following condition:

$$\frac{de}{d\alpha_i^k} = 0 \tag{1.11}$$

From the stated condition and equation 1.10 the following terms are reached.(See appendix for mathematical manipulations)

$$\alpha_n^k = T_{mn}^{-1} b_m \tag{1.12}$$

Where:

$$T_{mn} = \int_{\Omega} |\Phi_n(x)|^2 |\Phi_m(x)|^2 dx \tag{1.13}$$

$$b_m = \int_{\Omega} g^k_{exact}(x) |\Phi_m(x)|^2 dx \tag{1.14}$$

1.2.2 Higher-Order Mode Theory in Electromagnetic Domain

When it comes to the electromagnetic counterpart resonator of doubly clamped beam resonators in mechanical domain, a similar theory can be engendered by the same approach in microwave regime. In the aforementioned studies the writer of the thesis spent effort to explain the paradigms exploited in the microwave sensors. Nonetheless, among these paradigms only a minute portion of efforts spent in higher-order modes approach whereas this approach is shown to have advanced capability in sensing applications. For example, single molecule weighing in real time, measuring mass and stiffness of the analytes simultaneously and obtaining spatial information are just the ones that come in forefronts. Thus our research topic derives from this absence and applicability in microwave domain, the exploitation of higher-order modes in microwave resonators.

The higher-order mode sensing theory in NEMS is valid for any resonator in any domain so long as structure can provide a measurable frequency shift and has definite resonant mode shapes. Therefore the electromagnetic counterpart of the NEMS resonator emerges as microwave resonators of any kind such as microstrip TL, coplanar waveguide, split ring or cavity resonators. Indeed, it is crucial to choose a structure which can easily be integrated with a microfluidic channel since the purpose of this application is to make biological analyses.

In dielectric impedance sensing, a small analyte that passes through the embedded microfluidic channel induces a frequency shift in the resonance as follows

[24], [25], [26]:

$$\delta f_n = \frac{f_n' - f_n}{f_n} = -\frac{\int_{V_0} \triangle\epsilon(r) E_n^2 d^3r}{\int_{V_0} (\epsilon(r) E_n^2 + \mu(r) H_n^2) d^3r} \tag{1.15}$$

where f_n and f_n' are the resonant frequency and shifted resonant frequency due presence of analyte respectively, $\epsilon(r)$ is the dielectric constant of the medium, $\mu(r)$ is the permeability of the medium, E_n is the electric field, H_n is the magnetic field, $\triangle\epsilon$ is the permittivity difference between the medium and the analyte that replaced the medium with its presence. The term $(\frac{\triangle f_n}{f_n}) = \delta f_n$ is defined as the fractional frequency shift. The denominator of the equation 10 is the total energy stored in the resonator and harmonic oscillator property ($< \int_{V_0} \epsilon(r) E_n^2 d^3r > = < \int_{V_0} \mu(r) H_n^2) d^3r >$) is valid at resonance. With the overall strength of the electrical field E_n, equation 10 can be restated as:

$$\delta f_n = -\frac{1}{2} \frac{\int_{V_0} \triangle\epsilon(r) |\phi_n|^2(r) d^3r}{\int_{V_0} \epsilon(r) |\phi_n|^2 d^3r} \tag{1.16}$$

At this point reader should notice the similarity between the equations 1.4 and 1.15. The areal mass density $\mu(r)$ is replaced by the change in dielectric $\triangle\epsilon(r)$, both denominators are volume integrals, mode shapes take place in the same fashion and even the $-1/2$ fraction is present in the forefront. Now recall the definition of mass of the device in mechanical domain: $\int_\Omega \rho_{dev} |\Phi_n|^2 dV = M$. At this stage again, there is a very similar term which is called the electrical volume of the device for the n_{th} mode is defined as:

$$V_n = \int_{V_n} \epsilon(r) |\phi_n(r)|^2 d^3r = \Omega_{res} \tag{1.17}$$

In the electromagnetic domain, the moments we seek for information belongs to function $\triangle\epsilon(r)$. Similarly, the geometric moments of the function are taken with the functions $g(r)^k = r^k$. Indeed these functions can be expressed as the linear combinations of the unperturbed mode shapes as follows:

$$g^k(r) = \Sigma_n^N |\Phi_n(r)|^2 \tag{1.18}$$

The counterpart of the surface loading term F_n is the excess electrical volume of the analyte. The frequency dependency of the permittivity is included in the expression by adding a correction term to be determined according to the frequency is defined as $\mu(\omega)$ and multiplied with the difference of dielectric constant.

$$v_n = \int_{V_0} \triangle\epsilon(r)\mu(\omega)|\Phi_n(r)|^2 d^3r \tag{1.19}$$

Consequently we can state the following equation by combining 1.17 and 1.16:

$$v_n = -2\Omega_{res}\mu(\omega)\delta f_n \tag{1.20}$$

Therefore it can be confidently stated that the moments of the permittivity difference function can be linked to the frequency shifts as follows:

$$m^k = \int_{V_0} \triangle\epsilon(r)\mu(\omega)g^k(r)d^3r = \Sigma_n^N \alpha_n^k \int_{V_0} \triangle\epsilon(r)\mu(\omega)|\Phi_n|^2 d^3r = \Sigma_n^N \alpha_n^k v_n \tag{1.21}$$

In conclusion we can write the moment of the $\triangle\epsilon(r)$ related to the experimentally obtained frequency shifts as it was written in mechanical domain as follows:

$$m^k = -2\Omega_{res}\mu(\omega)\Sigma_n^N \alpha_n^k \delta f_n \tag{1.22}$$

The higher order moments are taken just as they were taken in mechanical domain and weighting coefficients are reached through the same least squares method. Nonetheless, their derivation can be seen in appendix section.

1.3 Point Particle Approximation

The scope of this thesis does not extend to information extraction via modes higher than the second one. Therefore in our research -which is only the sliver of the upcoming phases- the researchers focused on two mode applications with point particle approximation. With these application the position and excess electrical volume of pipetted analytes, water droplets and cells are measured with point particle approach. For clarity, equation 1.16 is rewritten with V_n term in the denominator as follows [27].

$$\delta f_n = -\frac{\int_{V_0} \Delta\epsilon(r)|\phi_n|^2(r)d^3r}{2V_n}$$

In this method equations are same up to the equation above. After that line, the following approximation is made which is the basis of point particle approximation.

$$\Delta\epsilon(r) = \nu\delta(r - r_p) \tag{1.23}$$

Where r_p is the position of the particle and ν is the total excess electrical volume of the particle. Since the thickness of the microstrip signal line is small and fringing fields can be neglected, the microstrip TL resonator can be claimed as a one dimensional resonator as the doubly clamped beam NEMS resonators. Henceforth, due to the presence of dirac-delta function, only a sample point comes out from the integral which results in the following equations for the first two modes.

$$\delta f_1 = -\frac{\nu}{2V_1}\phi_1^2(x) \tag{1.24}$$

$$\delta f_2 = -\frac{\nu}{2V_2}\phi_2^2(x) \tag{1.25}$$

For a one dimensional resonator shorted at both ends considering the fringing fields can be neglected, the electric field in the entirety can be expressed as $E_n = A_n\phi_n(x)\hat{\mathbf{k}}$, where the amplitude A_n was dropped in the previous manipulations. Therefore it is fair to express the mode shapes are as follows.

$$\phi_n = sin(n\pi x) \tag{1.26}$$

The equations 1.24 and 1.25 establishes a linear system of equations with 2 unknowns that would result in a unique solution thanks to the orthonormal mode shapes and disparate frequency shifts as follows.

$$\begin{bmatrix} \delta f_1 \\ \delta f_2 \end{bmatrix} = \begin{bmatrix} -\frac{1}{2}\frac{\nu}{V_1} & 0 \\ 0 & -\frac{1}{2}\frac{\nu}{V_2} \end{bmatrix} \begin{bmatrix} \phi_1(x)^2 \\ \phi_2(x)^2 \end{bmatrix} \tag{1.27}$$

The δf_1 and δf_2 values are obtained experimentally, V_1 and V_2 can be calculated according to the geometry after the resonator is manufactured. Thus, the system can be solved for spatial coordinate x, then from either of the equations 1.24 or 1.25, the excess electrical volume ν can be calculated.

Chapter 2

Feasibility Studies

In this chapter the writer of the thesis focuses on the choice of microwave resonators applicable for higher-order mode theory, the simulation results, first generation experiment paradigm and experimental verification of the theory. In the last part of the section the predecessor of our latest experiment paradigm which is droplet experiments in real time will be explained and the cell measurement scheme will be introduced. a

2.1 Preliminary Information on Microwave Resonators

In the aforementioned sections it is stated that any microwave resonator with mathematically definite mode shape can be tailored into the higher-order mode theory. Nevertheless, as a starting point choosing the optimum resonator is crucial in terms of ease in manufacturing, measurement and adapting it for biological applications. When considering the stated criteria of three, a microstrip transmission line resonator is a sensible choice when its structure, connection to the outside world and distribution of electrical field is considered.

A microstrip transmission line is a three part structure composed of a conductive signal line, conductive ground plane and a dielectric filling layer as well as the electric field distribution in a random cross section in the line can be seen in figure 2.1. Besides, if a transmission line is terminated with a short at the load side and if the total length of the TL is half of the wavelength at a specific frequency resonance occurs. This kind of TL resonators are called short-circuited $\lambda/2$ line resonators. The voltage profile of $\lambda/2$ resonators for the first two modes are shown in figure 2.1. It is important to emphasize that the both voltage profiles have minima at the short boundary conditions since at zero impedance voltage is zero whereas the current is infinity.

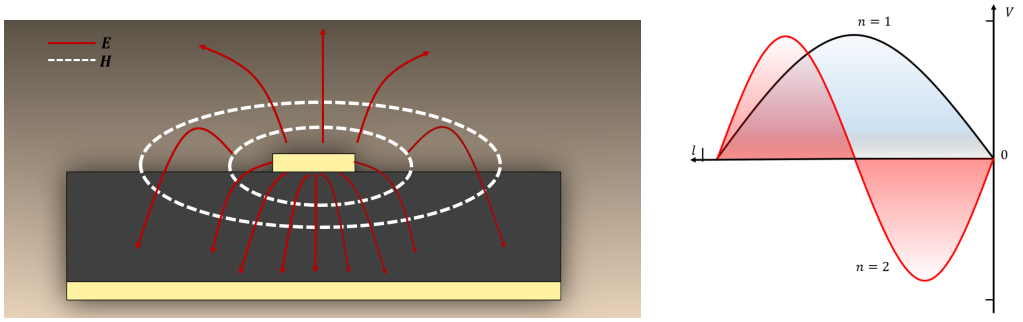

(a) Electric and magnetic field distribution in a cross-section of a microstrip TL

(b) Voltage profile along a microstrip TL resonator

Figure 2.1: Microstrip TL characteristics

For application of higher-order mode theory in electromagnetic domain, microstrip TL resonators have conspicuous aspects. Recall that in the mechanical domain doubly clamped beams which have stagnant boundary conditions hence pure sinusoidal mode shapes at resonance. The shorted transmission lines also can be claimed to have stagnant boundary conditions in terms of electric field at their terminals. Therefore they have pure sinusoidal mode-shapes and can be exploited as 1-D resonators as doubly clamped beam NEMS were in mechanical domain. This statement can be seen with clarity in figure 2.2. In here, the simulation results of a microstrip TL resonator whose boundary conditions are defined as shorts in COMSOL environment and simulations were for eigenfrequencies of the structures. The resulting first four consequent resonant mode-shapes can be

seen below.

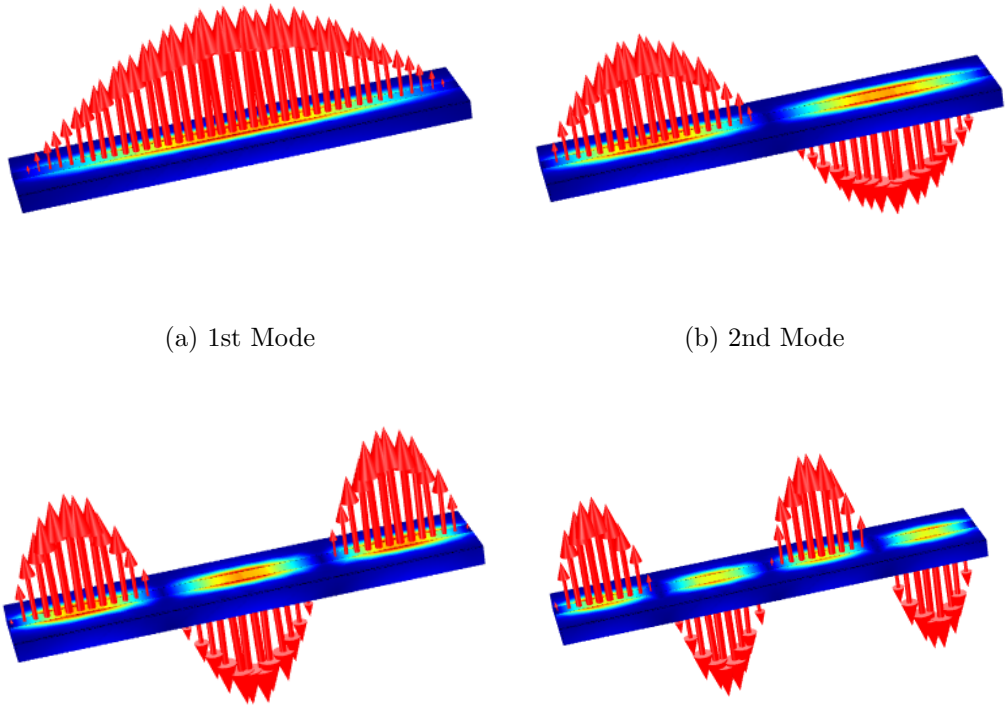

(a) 1st Mode

(b) 2nd Mode

(c) 3rd Mode

(d) 4th Mode

Figure 2.2: First four consequent mode shapes of a microwave TL resonator

After reaching this simulation results, it is shown that microstrip TL resonators can have pure sinusoid mode-shapes henceforth are good candidates for higher-order mode sensing theory. The frequency shifts due to presence of an analyte along the line causes frequency shifts related to their position. For instance for the first mode, at the normalized position 0.5 which corresponds to the midst of the structure, an analyte induces the maximum frequency shift since at that location the first mode has its maximum in terms of electric field. Where as this position is 0.33 for the second mode and so on for the other modes.

According to the observations on these simulations, it is also seen that the most of the electric field is sandwiched between the two conducting plane. Therefore

for sensing applications, it is sensible to define the sensing region as the volume between the two analytes.

2.2 FEM Simulation Studies

2.2.1 Microstrip Simulations

In our simulation endeavors first it is ensured that the frequency shifts due to presence of particles occurs with respect to position and mode shape. This means that each particle with exact same amount of volume causes frequency shifts in ratio with the mode shape. The simulations are run in a certain paradigm to eliminate frequency shifts comes from the discretization of the model. Therefore, first 49 particles -which are cubes of $100um$-separated by 1mm distance are placed in the microstrip transmission line model which is shorted at both ends. First, only the dielectric material is assigned to each of the particles and simulation is run to obtain a reference frequency without shift. Then, starting from the leftmost particle and keeping the mesh same at each run, water material is assigned to particles one by one. The frequency shifts are taken from the comsol and plotted with respect to their normalized position in Matlab. Furthermore, the theoretical expected frequency shifts with respect to mode shapes are also graphed on the same plots for the first two modes.

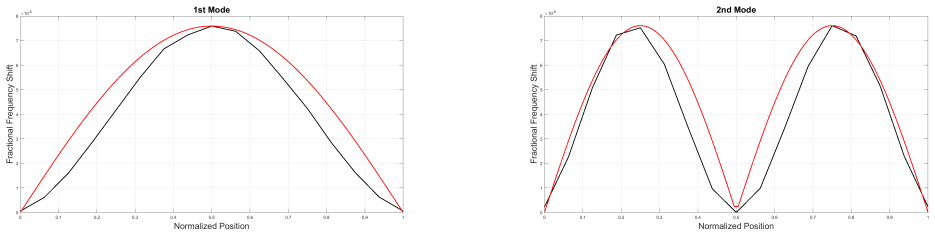

(a) 1st Mode (b) 2nd Mode

Figure 2.3: Frequency shifts and theoretical shifts with respect to mode shapes for the first two modes

After this initial simulation, simulations with much more intense meshing on a supercomputer are run. This is because since in FEM simulations, the discretized model and environment cause uncertainties and lowers the accuracy of calculations.

Microstrip based microwave sensor is modeled on COMSOL environment as follows. Substrate of the microstrip transmission line is chosen to be glass (ϵ_r = 4.2) of 0.6mm height, 3mm width and 50mm length. Since the transmission length is small, conduction and impedance losses are negligible. Upper conductor and ground plane are defined by using perfect electric conductor boundary condition (width of the upper conductor is 1mm). To realize the $\lambda/2$ shorted transmission line resonators, a uniform rectangular lumped port boundary condition with excitation is defined on one end of the microstrip (lumped port on COMSOL is an approximation of the coaxial cable). On the other end we defined a rectangular area same as the previously defined lumped port's area, as perfect electric boundary condition which is in touch with upper conductor and ground plane so that the microstrip is shorted on one end. To operate in the most uniform Electrical field within the cross-section of the channel, sensing line is aligned with the upper conductor. A cylindrical microchannel of 100micron diameter is defined and its lateral axis is aligned with the central axis of the upper conductor. The carrier fluid is chosen as water. Sample particles are defined as $20\mu m$ sided cubes and placed within the microchannel. Material choice for the particles is oil of relative permittivity 2.5 which is close to the substrate material choice of glass. Microstrip transmission line is surrounded with an air box. The outer faces of the air box are defined as scattering boundary condition to eliminate/minimize the interference of the reflected waves. To get the most accurate results, we used the highest mesh option of extremely high mesh on our model and run the simulations on a supercomputer. In this mesh option, the smallest element size turned out to be 90 microns and resulted in a DOF number of 2.5 millions. Since the smallest change in meshing can reflect itself as a frequency shift, we run the simulations for each position twice and hold the meshing the same. The defined particle volume is filled once with a carrier fluid ($\epsilon_{r,water} = 78.3$), once with a material of interest ($\epsilon_{r,oil} = 2.5$). In this way, frequency shift caused by the presence of a particle in

a continuous flow, is obtained as a snapshot of the flow.

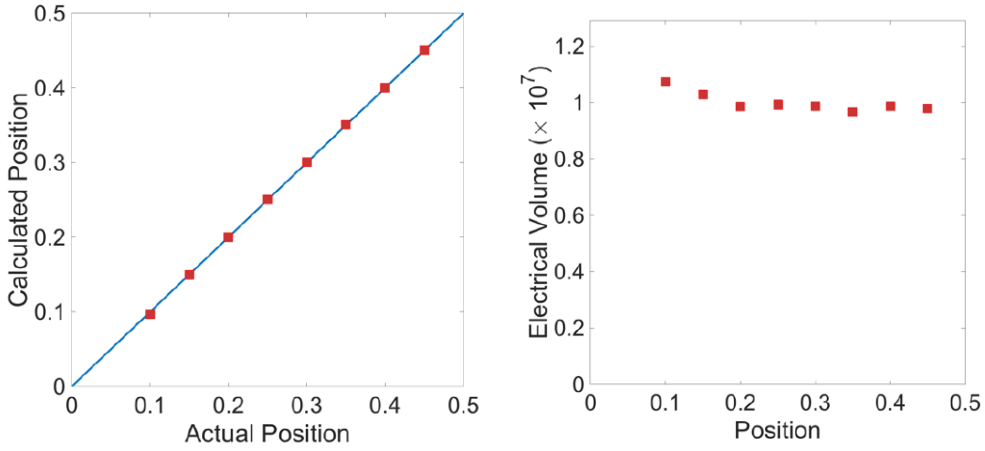

(a) Obtention of particle position by frequency shifts

(b) Obtention of electrical volume of generated particles

Figure 2.4: Simulation results

2.2.2 Ring Resonator Simulations

Ring resonator structures have intriguing properties such as their negative refractive indices [28], being left handed structures [29], high quality factors, adjustable transmission characteristics [30] and so on. Compared to microstrip resonators they can be made electrically small [31], [32],they can be bestowed with multigaps that may be exploited as mirofluidic channel implementation [33],

In terms of mode shape of the resonator and applicability to the higher-order mode theory, microstrip resonators provide more than sufficient results. Nevertheless, the ring resonators have their on fame for high quality factors and more definite mode shapes. This is because, to ensure pure sinusoidal modeshapes, the both ends of microstrip resonator are terminated with shorts. To short an end of a transmission line a finite amount of physical connection is required. According to the operating frequency, this amount of short connection can behave as an inductor or capacitance in reality, hence disrupts the mode shapes and induces noise. Since ring resonator structure does not need shorts to have definite mode

shapes and has popularity in bio-applications, another feasibility study is run on these structures.

To simulate such a structure, first a model is designed on Solidworks environment, then the sketch is opened in Comsol simulator. The designed ring has inner and outer radii as $r_o = 8mm$ and $r_i = 7mm$. Two connector extensions to couple the resonator is also implemented in the system. As a substrate the silicon of permittivity 11.7 is chosen. According to these the mode shapes and resonant frequencies come up as follows.

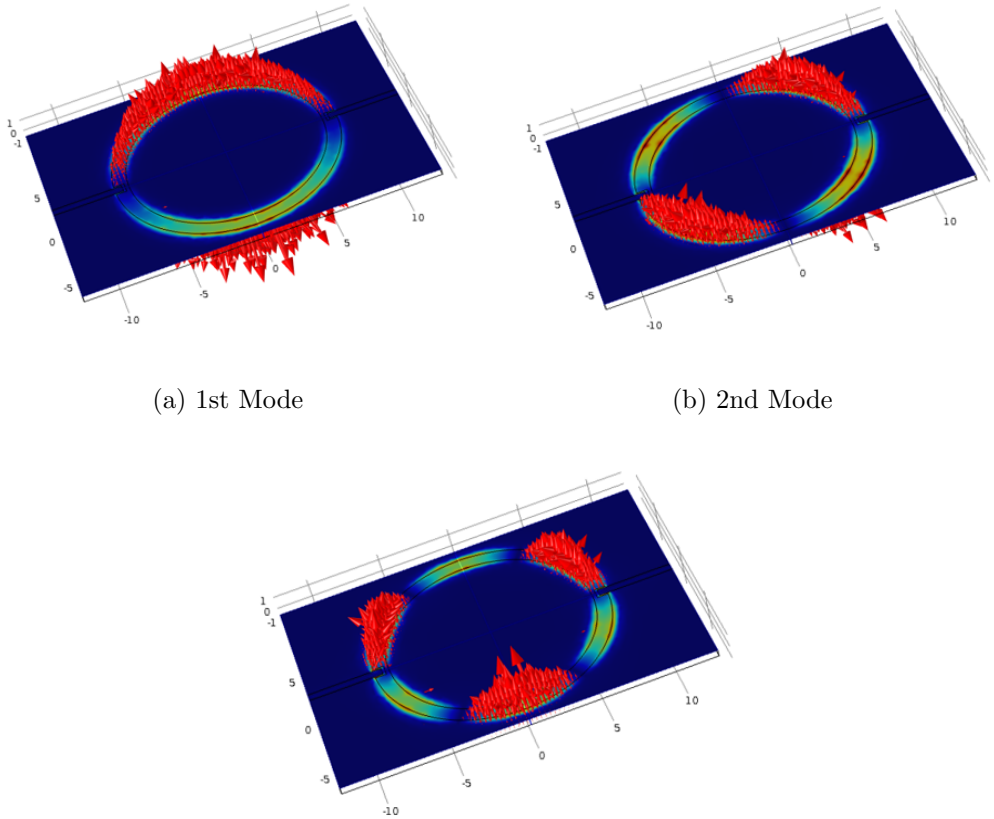

(a) 1st Mode

(b) 2nd Mode

(c) 3rd Mode

Figure 2.5: First three consequent mode shapes of a ring resonator

As it can be seen, the upper half and lower half of the resonator behaves like two separate and bent microstrip TL resonators with sinusoidal mode shapes. Since

the structure has definite mode shapes, it can be employed in higher-order mode theory. As an initial step, the particles -which are cubes of dimension $100\mu m$- are placed in the arc which is the midst of the upper signal line separated by an equidistance of 18°. To have a reference resonance frequency, all the materials are filled with the same material as the substrate. Then a simulation is run for each -an ensemble of 9 simulations- particle so that the induced frequency shift by the particle with respect to its location is reached. Also by this paradigm, simulations are run without changing the mesh, henceforth the frequency shift due to different discretization of meshing is avoided.

Below in the figure, it can be seen that the frequency shifts occurred with respect to the mode shape. The particle which is located in a place where the strength of electric field is high induces greater frequency shift whereas in the opposite case induces a little frequency shift.

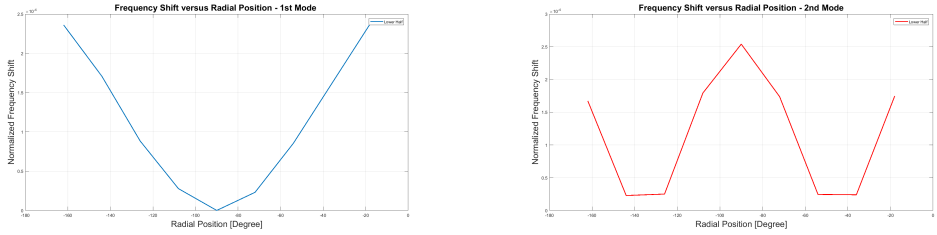

(a) 1st Mode (b) 2nd Mode

Figure 2.6: Simulated frequency shifts due to particle presence in a ring resonator

Moreover, with a simple transformation between cartesian and polar coordinates, position calculation through the simulated data is realized. The results are pretty much the same as it was in the microstrip resonator case. The maximum error percentage in this case is 48% percent, however within the 54-126° interval of the resonator the error level do not exceed 3% which is competitive with the microstrip resonator application.

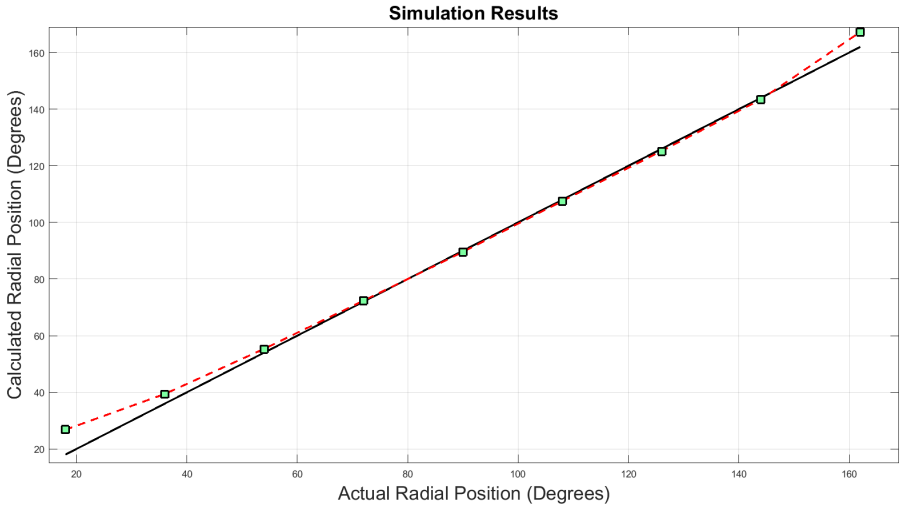

Figure 2.7: Angular position calculation with experimentally obtained frequency shifts in ring resonator case

At this stage, an expected pure sinusoidal mode shape is not fitted and plotted on the simulated frequency shifts since a mathematical representation in terms of sine functions are not tailored into the theory. This is because ring resonator structure are not further used in our studies yet a preliminary research on them are realized. Nonetheless, it is shown by that when an experimental setup is installed and pipette experiments are conducted on this structure, as they were realized for microstrip TL resonators, it is shown that the experimental frequency shifts matches these simulated ones. As a deduction, this structure can be further examined and used in higher-order mode theory.

2.3 Experimental Verification of the Theory

2.3.1 Microstrip Transmission Line Resonator Case

After getting promising results from the simulation studies, an initial experimental verification of the proposed theory is run. According to this, a similar

structure that we modeled on COMSOL environment is designed and produced on printed circuit board (PCB). The designed PCB is 102 mm long has 2 mm signal line width and has 9 equidistant through holes of 1.2 mm diameter and with mm separation. The loci of the holes are at 11: 10: 91 mm. The dielectric material of the PCB is FR4 whose relative permittivity is 4.3 and as analyte glycerin is employed whose relative permittivity is approximately 60.

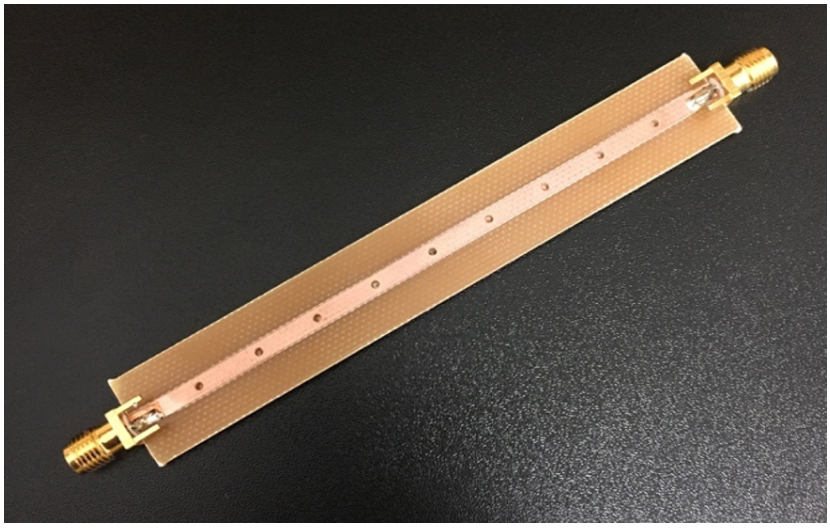

Figure 2.8: The PCB resonator with drilled holes used in pipette experiments

The scheme of the experiment is as follows. The experimentalist records the resonance frequencies of the first two modes initially then fills the first hole with an analyte using a precision pipette. After filling the hole, resonance frequencies are recorded again from the Spectrum Analyzer (Keysight CXA n9000a). Before filling the next hole, the previous hole is emptied with pressurized air and another measurement is taken to form a reference for the consequent measurement. In this way, each frequency shift is defined for its own datum to eliminate the shifts of due to residual analytes in the precursory holes.

The main sources of uncertainties in this experiment are it is not possible to fill the holes with the exact same amount of analytes and purge the holes for next hole's measurement. Therefore the frequency shifts due to analyte presence does not induce fully position dependent frequency shifts.

According to the experiments the position dependent frequency shifts as a function of analyte position emerges as follows. The frequency shifts profile along the entirety of the structure is not smooth as they were in the simulations regarding the mentioned uncertainty factors.

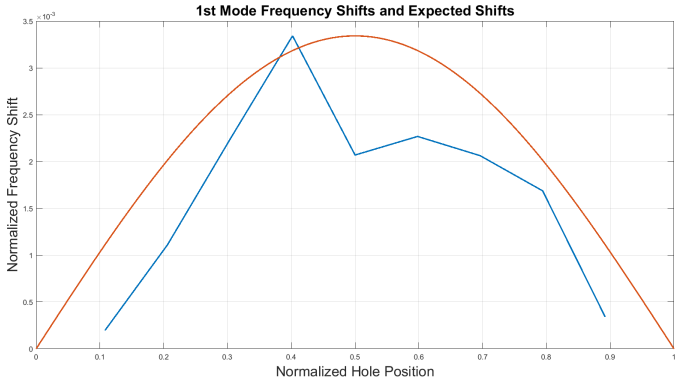

(a) Expected frequency shift profile and experimental frequency shift for the 1st mode

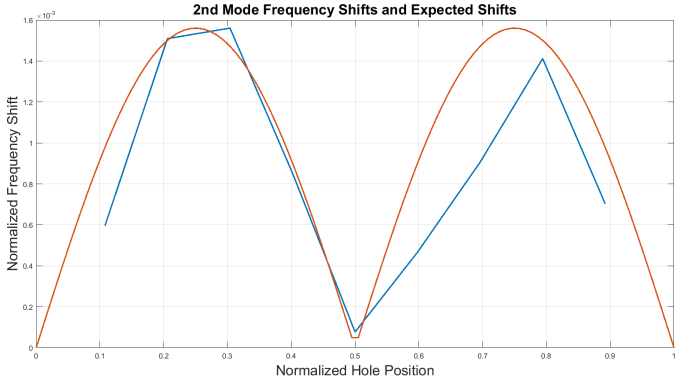

(b) Expected frequency shift profile and experimental frequency shift for the 2nd mode

Figure 2.9: Frequency shift profile

The experimentally obtained frequency shifts are used in our theory for calculation of the position of the pipetted analytes. Their exact position are pre-known since the holes are punched into the PCB according to the design. The obtained results are promising as they were in the simulations. The maximum error percent obtained in the experiments were 14%. It is important to emphasize the

only one half of the structure must be exploited as sensing region due to the nature of the *arccos* function. And this function supplies the most accurate results within 0.2-0.45 normalized position band. The percent error in this interval did not exceed 3 % even though the uncertainty sources mentioned previously.

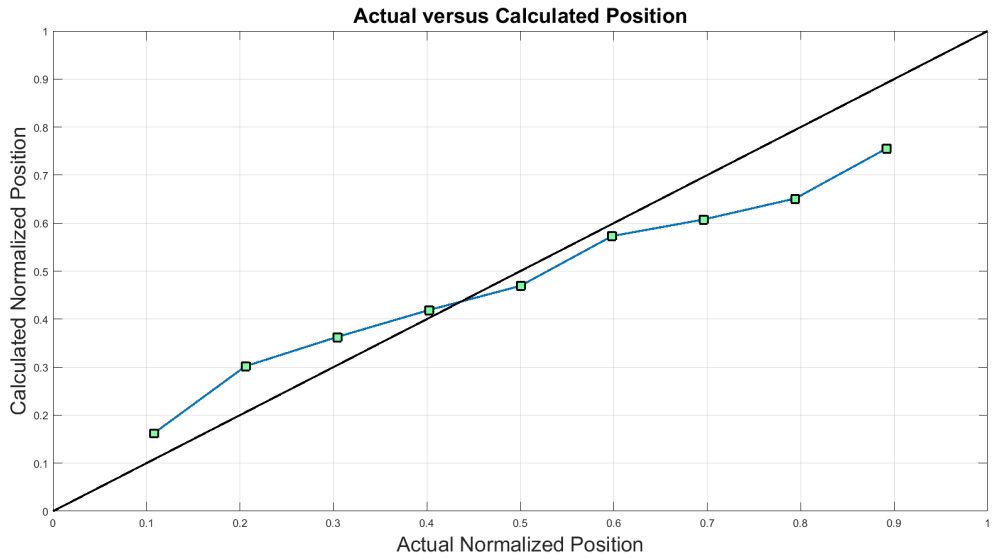

Figure 2.10: Position calculation through experimentally obtained frequency shifts

2.3.2 Ring Resonator Case

The same kind pipetting analytes experiment is conducted on the ring resonator structure. The radial location of holes on the structure are positioned just as they were in the simulation case, which is 18°:18°:162°. Once again, the experimentally obtained frequency shifts matches the ones coming from the simulations as they can be seen below in the figure.

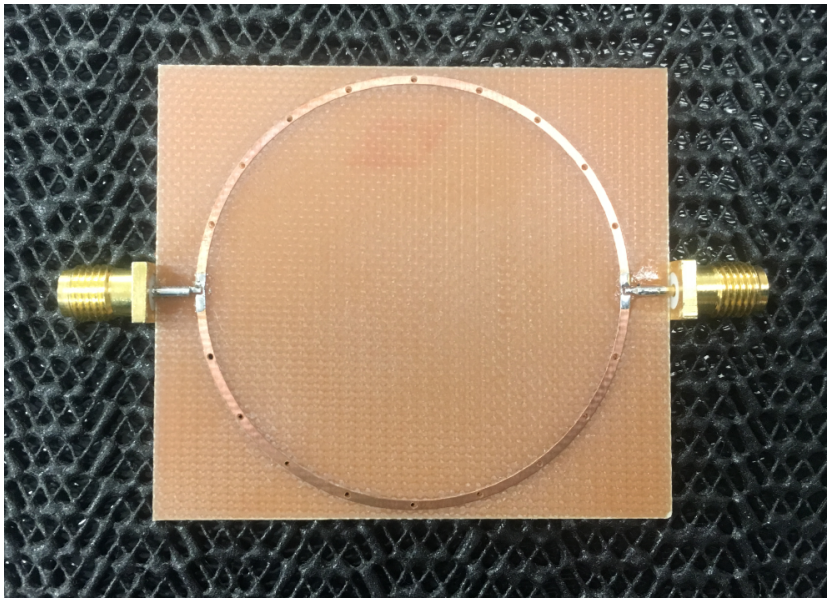

Figure 2.11: The PCB ring resonator with drilled holes used in pipette experiments

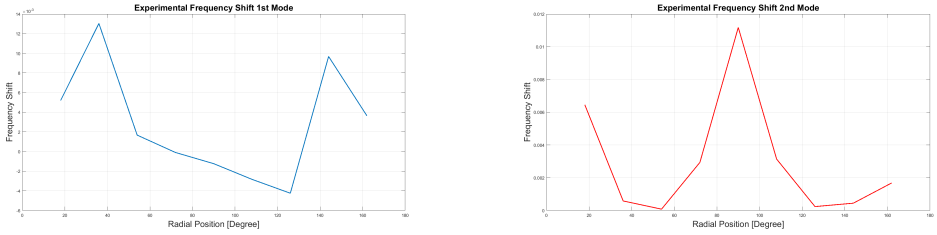

(a) 1st Mode (b) 2nd Mode

Figure 2.12: Experimental frequency shifts due to analyte presence in a ring resonator

The same sources of uncertainties in the microstrip case reiterates here which are placing the exact same amount of analyte with a syringe, emptying the hole totally before next step of measurement and the finite number of holes give dispersed results. The results is not as satisfying as it is given in the simulation case. This is because, there is a simple transformation is realized as follows. First the ring resonator is transformed in to a linear resonator and the position of analytes are determined from the frequency shifts on the virtual straight line resonator.

Second, the transformation is undone to locate the analytes on the ring structure. During this operation a certain amount of uncertainty added to the calculation. And considering the significant digits that can be extracted from the signal analyzer during pipette experiments, the experiment does not give successful results as it was in the straight microstrip case. The experiment must be repeated with a smaller ring resonator with larger holes to induce greater frequency shifts. Also, if the experiment is repeated with vector network analyzer which can supply greater significant digits at higher frequencies will be beneficial.

2.4 Deductions and Further Steps

Until this subject, the preliminary information on two microwave resonators are given, the simulation methodology, initial results regarding the frequency shifts, electrical volume and position are provided and it is shown that microstrip TL resonators and microwave ring resonators are fit for higher-order mode application. Since the manufacturing of the microstrip TL are easier than the ring structure and because their mode shapes can be defined mathematically by pure sinusoid functions they are chosen for next generation experiments. In the next phases of the research, the pipette experiments are evolved to the real time measurements thanks to the embedded microchannels and continuous fluid flow that hosts droplets and cells within the microstrip TL resonators where the electric field has strong intensity.

Chapter 3

Experiment Methodology

In this section first, a microwave electronics background for the enthusiastic reader will be established. All the necessary equipment, their capability, resolution, programming and limits will be explained. Then the built experimental setup for real time measurements and control scheme will be explained.

3.1 Why Microwave Electronics Differ from the Standard Circuit Theory?

Microwave electronics considers the systems that operate in high frequencies in the interval of 300 MHz and 300 GHz. In this regime the wavelengths are in between 1m and 1mm, not in the microscale, hence the name can be misleading. What makes microwave electronics require a special treatment is just because of these wavelength range. In standard circuit theory, the frequencies and components allow engineers to employ a lumped element model. For instance, in the kHz regime one can state that the voltage difference between two points along a wire is zero. The reason behind this approach relies on the success of an approximation. Because the wavelength of the signal passing through the circuit is much larger than the physical length of the circuit we do not encounter significant

phase differences along the transmission lines so that we can apply the lumped element model.

When the subject of interest is high frequencies this approach is no longer valid since the wavelength of the signals in this regime can be much smaller than the circuit itself. As a result, within the extent of a circuit or a component, significant phase differences can be observed. Even the impedance of a microwave signal carrying TL is not constant along its extent. Hence a distributed element approach based on Maxwell's electromagnetic equations is employed. This approach encompasses all the electric and magnetic properties of the medium such as permittivity, permeability, conductivity, skin depth, direction of propagation, propagation constant and so on.

Practically, microwave electronics has some unique properties when compared to low frequency circuits. For instance as we all know, Kirchoff Laws apply for closed loop circuits and indeed if a circuit is not closed it is completed thus it does not work. This may not be the case in microwave electronics. A transmission line(TL) may be left open for the purpose of impedance matching, a structure might be shorted to make a resonator, a minute TL piece might be left alone somewhere along the circuit to create a capacitance, a TL might be intentionally meandered so that a certain degree of phase is reached, between two parallel wires a resistance may be placed to isolate these two lines although it may resemble a short at first, two consecutive signal carrying TLs may not be in touch which may be seen as an open at first sight yet they do communicate because of wave propagation and so on. Therefore, constructing a frame of mind that every voltage and current in these circuits are travelling or stagnant waves -but waves- can be helpful.

Although standard circuit theory and microwave electronics are two distinct disciplines, this does not mean that they never intersect and analogies can not be established. A beautiful example that would provide insight about wave propagation along the TLs and bring the two together are Telegrapher's equations. A transmission line is a distributed-parameter network and they always include at least two conducting lines, yet lumped-element circuit model can be employed for

its mathematical realization. Below, you see a differential length of a TL where:

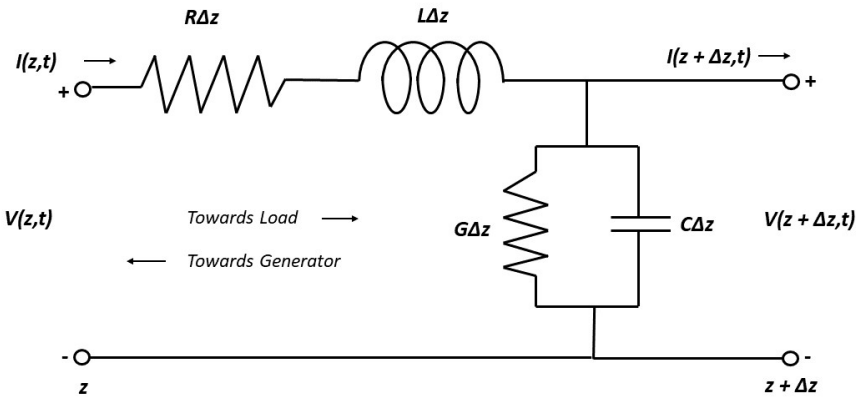

Figure 3.1: A differential length of a transsmission line

R: Series resistance per unit length, Ω/m **L:** Series inductance per unit length, H/m **G:** Shunt conductance per unit length, S/m **C:** Shunt capacitance per unit length, F/m

The series inductance stands for the self inductance between the two conductors, shunt capacitance is present because of close proximity of the two conductors, the series resistance is due to the finite conductivity of the metals and shunt conductance is due to dielectric loss in the material and fills the gap between the conductors.[Pozar]

Within this finite length of TL we can apply Kirchhoff's voltage law as follows (notice the position and time dependence of voltage and current):

$$v(z,t) - R\Delta z i(z,t) - L\Delta z \frac{\partial i(z,t)}{\partial t} - v(z+\Delta z,t) = 0$$

In the same segment, Kirchhoff's current results in:

$$i(z,t) - G\Delta z v(z+\Delta z,t) - C\Delta z \frac{\partial v(z+\Delta z,t)}{\partial t} - i(z+\Delta z,t) = 0$$

Dividing both equations above by Δz and taking the limit as $\Delta z \rightarrow = 0$ results in the following differential equations:

$$\frac{\partial v(z,t)}{\partial z} = -Ri(z,t) - L\frac{\partial i(z,t)}{\partial t}$$

$$\frac{\partial i(z,t)}{\partial z} = -Gv(z,t) - C\frac{\partial v(z,t)}{\partial t}$$

For the steady-state condition with sinusoidal signals, the equations become further as follows:

$$\frac{dV(z)}{dz} = -(R + j\omega L)I(z)$$

$$\frac{dI(z)}{dz} = -(G + j\omega C)V(z)$$

The two equations can result in two independent second order homogenous differential equations that provides travelling wave solutions of voltage and current as follows:

$$\frac{d^2V(z)}{d^2z} = -\gamma^2 V(z) = 0$$

$$\frac{d^2I(z)}{d^2z} = -\gamma^2 I(z) = 0$$

Where $\gamma = \sqrt{(R + j\omega L)(G + j\omega C)}$ is the complex propagation constant. Finally travelling wave equations in a tranmission line are as follows:

$$V(z) = V_o^+ e^{-\gamma z} + V_o^- e^{-\gamma z}$$

$$I(z) = I_o^+ e^{-\gamma z} + I_o^- e^{-\gamma z}$$

The superscripts + and − denotes for the incident and reflected waves. This phenomena can give many insights about why impedance -$Z = V/I$- varies along a TL, phase shift occurs along the extent of a TL, two conductors are needed in a network, a TL can be operational eventhough it has a short or open somewhere along the length, it is possible to excite a line without making a physical connection, possible to read out a signal even by probing it through a distance or standing wave patterns occur due to some certain boundary conditions.

3.2 Electronics Background

In this subsection the required microwave components and their working principles will be explained briefly. The objective is to give an insight to the user about the measurement circuitry and give practical information about microwave electronics to the novice mechanical engineers who just started to their m.sc. degree. The field itself and the systems that operate in microwave regime could be intimidating at first sight, however embracing the problem and knowing that everything is a different approach of mathematical modeling can be a relief.

Power Divider

A power divider is a passive component used to divide power that enters the source port of the network and distribute it equally between the output ports. For instance, a 2-way Wilkinson power divider takes the signal from its source port within its frequency band and splits into two signals of equal amplitude (3dB

reduction). If the device is connected in a reversed manner, it combines the two signals at its source port, thus it is also called a power combiner. They can be made with arbitrary power division, however in this research equal split(3db)3 port, isolated and 0° power dividers are employed.

RF Mixers and Frequency Conversion

RF mixers are the key components in transmitters, receivers, heterodyne signal processing, downmixing(downconversion) and upconversion. It is a passive and nonlinear device comprised of 3 ports that can be used for both down-conversion and up-conversion. In our application mixers are used for both downconversion and upconversion to provide a readable signal for the lock-in amplifiers which will be explained in detail later on. Mixers for down-conversion are operated as follows: A radio frequency that is desired for down-conversion is supplied to the RF port [34]. In the other port a signal which is called local oscillator (LO) is multiplied with the RF frequency as mathematically explained below.

$$V_{IF}(t) = KV_{RF}(t)V_{LO}(t) = Kcos2\pi f_{RF}t.cos2\pi f_{LO}t$$
$$= \frac{K}{2}[cos2\pi(f_{RF} - f_{LO})t + cos2\pi(f_{RF} + f_{LO})t]$$

According to the simple trigonometric identity given above, the output of a mixer is the sum and difference of the RF and LO frequencies. For down-conversion the high frequency component is filtered out thus the RF frequency is converted to the difference of the two frequencies. The figure below is beneficial in illustrating this process.

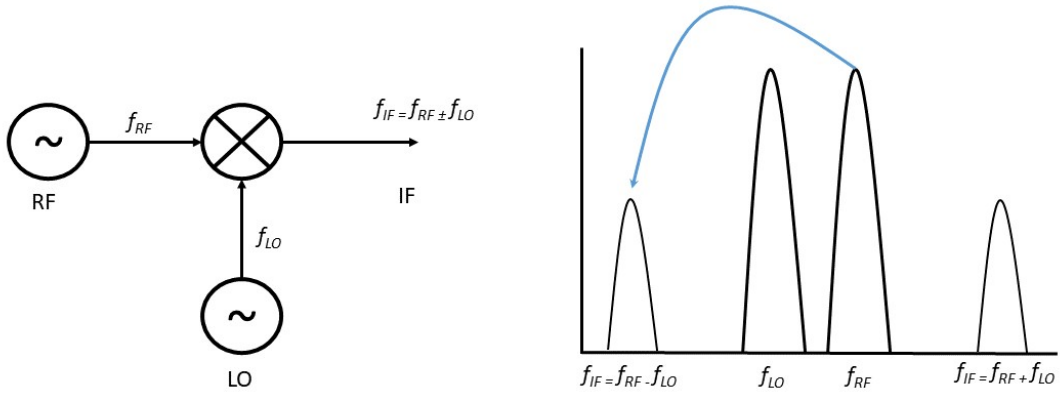

Figure 3.2: Downconversion with a mixer.

The procedure in upconversion is almost the same as it is in the downconversion [34]. The frequency for upconversion is supplied to the IF port whereas the LO port is a again a pure sine tone or a square wave. When the LO signal has a high voltage value the mixer can be considered ON when the opposite is valid it is considered OFF. In this arrangement the multiplication of the frequencies are realized as follows:

$$\begin{aligned} V_{RF}(t) &= KV_{LO}(t)V_{IF}(t) = Kcos2\pi f_{LO}t.cos2\pi f_{IF}t \\ &= \frac{K}{2}[cos2\pi(f_{LO}-f_{IF})t + cos2\pi(f_{LO}+f_{IF})t] \end{aligned}$$

The illustration of this process can be examined below. Please take good note that this time the generated harmonics are much closer to the local oscillator signal henceforth a more careful filtering stage is needed to obtain solely the frequency of interest.

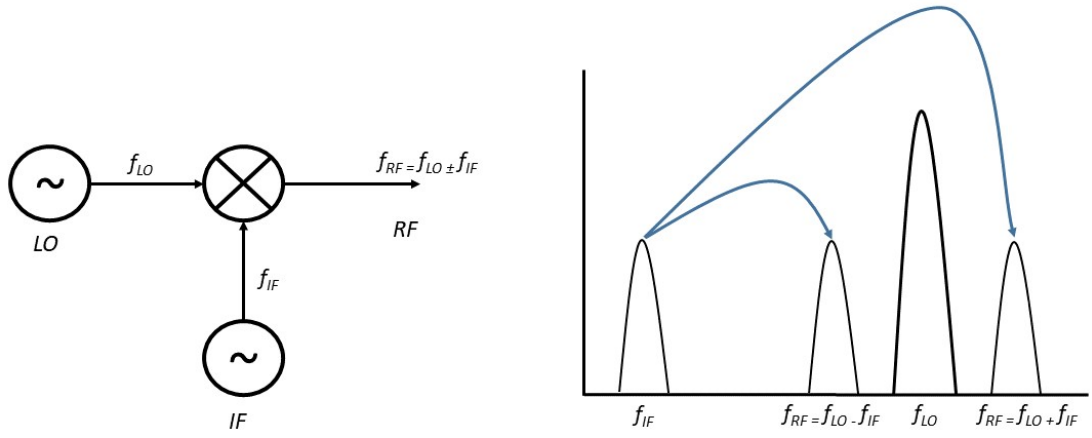

Figure 3.3: Upconversion with a mixer.

The upconversion and downconversion are vital for telecommunication applications. Since a 5% bandwidth of a high frequency signal carries much more information when compared to a low frequency signal, the information is upconverted first before sending. For instance, the antennas send information to very long distances and receivers catch them at some location. The antenna that sends information is called transmitter and actualizes upconversion. A receiver is another type of antenna that catches the sent information and donwconverts the signals to their original frequencies.

As a practical concern, apart from these two procedures and and the ports, the engineers must know some of the specifics of this component. First of all, since this is a nonlinear device one should not expect just 3 distinct and vivid frequencies at the output of the mixer. The most powerful ones are the harmonics expressed above yet the spectrum at the output of the mixer contains infinitely many harmonics although they have very little amplitude. Therefore the filtering stage after mixer must consider this fact.

The other noteworthy aspects are the type and level of the mixer, conversion

loss and 1dB compression point terms which are explained below.

Type of the Mixer: The high frequency output of the mixer is called upper sideband(USB) and the other one is called lower sideband(LSB). Not all of the mixers contains these two harmonics at their output. A single sideband mixer(SSB) contains only one of these two whereas a double-sideband(DSB) mixer contains both bands.

Level of the Mixer: Each mixer requires a certain level of power at their LO port for the diode within to saturate. For instance, in our experimental setup we have level 7 and level 10 mixers. For a level 7 mixer for example, one needs to supply at least 7dBm of power level at its LO port for device to perform normally.

Conversion Loss: As mentioned above, the result of the mixing process includes undesirable and infinitely many side harmonics. Since the energy conservation is valid for all type of systems it is valid for this operation too. The undesired side harmonics forms some of the total energy. And apart from this fact, there are losses due to imperfect impedance matching of the design energy losses occur. As a result the term conversion loss defines the imperfection in the frequency conversion processes and is defined as below.

$$L_c = 10log\frac{available\ RF\ input\ power}{available\ IF\ output\ power}$$

1dB Compression Point: After some power level according to the specifics of the device, the conversion loss is increased by 1dB although the input power is increased since the linearity of frequency conversion is ceased at this point. A significant indicator to keep in mind to remember the limits of the device and avoid to face abnormalities.

The writer of the thesis spend significant effort to explain the mixing and conversion processes in the mixer topic because they have the utmost importance

to comprehend the setup and develop it further.

Bias Tee

A bias tee is a simple L-C circuit is used to combine DC and RF signals. The configuration of the device is shown below. The inductor part of the device is connected to the DC source since a DC current will practically see a 0 ohm impedance since the impedance of of an indcutor is $Z_L = j\omega L$. The capacitor side of the device is connected to the RF source. The rf signal sees a small resistance against it since the impedance formula for capacitor is $Z_c = \frac{1}{j\omega C}$. As a result at the third port the DC and RF signals are combined and can be used for the application.

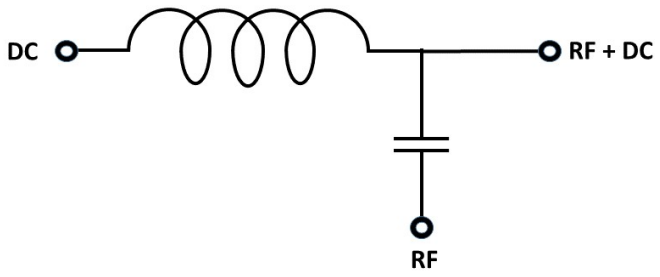

Figure 3.4: Bias-Tee

Amplifier

An amplifier is used to increase the amplitude of a signal. It is an active device which is the result of a careful impedance matching around a transistor so that the power loss across the device is minimum while increasing its amplitude by reaching a high forward transmission parameter S_{21}. Sometimes the amplification factor of a single amplifier is not enough. In those situations according to the required

amplification, the devices can be cascaded. However, one practical concern in such an endeavor is to put the amplifier with the smallest noise figure to the forefront. This is so because, as it can be seen in the formula below, the total noise figure of a cascaded amplifier network is the close to the noise figure of the first stage amplifier[34].

$$F_{cas} = F_1 + \frac{F_2 - 1}{G_{A_1}} + \frac{F_3 - 1}{G_{A_1} G_{A_2}} + ... + \frac{F_n - 1}{G_{A_1} G_{A_2} ... G_{A_{n-1}}}$$

Where F is the noise figure, G is the amplification factor mostly given in dB.

Since these are active devices, the connections has to be handled with care and with obeying a certain procedure as follows:

- Connect the load.
- Connect the DC connection.
- Release RF power.

RF Switch

A TTL driven RF switch is used to alternate the source signal between its rf output ports according to the frequency of the TTL signal. For instance, if the switch is supplied with a 1 Hz TTL signal, the source signal comes out from the port 1 for 1 second and 1 second from the port 2. In our application the role of the rf switch is to generate the LO signal for the mixers. The rf switch modulates the pumping signal of frequency ω_1 for the first mode by $\Delta\omega$ thus generates an output as $\omega_1 - \Delta\omega$ from one of its ports. Subsequently this LO

signal is multiplied by the ω_1 which is the RF signal. Upon this mixing, the output frequency is $cos(2\omega_1 t + \Delta\omega) + cos\Delta\omega$. The high frequency component is stripped of by filters from the spectrum and the low frequency component is sent to the input of the lock-in amplifier for reading.

Spectrum Analyzer

Spectrum analyzers are versatile devices used to characterize the frequency response of a DUT. According to the model, it sweeps a source signal between a determined frequency band in a very short time and reads out this signal after it comes out from the DUT so that the user can characterize the frequency response of the DUT. In our application we use a CXA keysight model spectrum analyzer to make an initial characterization of the resonators. According to the maxima in the spectrum we can address the location of the resonant frequencies to be used in open and closed loop measurements.

Signal Generator

Very elegant devices with very high frequency stabilities(up to $10e^{-11}$ allan deviation) with very low phase noises used to excite the DUT at determined frequencies. The pumping signal for fundamental modes of microwave transmission line resonators is generated through these devices.

Isolator

A perfect impedance matching within the entirety of the circuit may not be possible. If an impedance mismatch is present in the circuitry the waves that encounter different media reflects back and cause a lower signal to noise ratio. To avoid this issue, employing an isolator is a sensible choice.

Lock-In Amplifier

Among all the components and devices lock-in amplifier deserves a more elaborate explanation since it is the workhorse of our detection scheme and a critical part for myriad of applications. Lock-in amplifiers(LIA)are versatile equipments that can be used from nano scale engineering applications to space related physics researches. A lock-in amplifier has the ability to extract the full scale signal even if it is buried in a noise which is million times greater than the target signal.

A lock-in amplifier multiplies its input with a reference signal which is called heterodyne detection or down-mixing then performs a low-pass filtering to isolate the target signal from the noisy background and other signals that comprises the spectrum which is called phase-sensitive detection or demodulation. The reference signal(mostly a signal of sine form) is either generated within the LIA or provided externally for the LIA. The selective measurement and the term phase sensitive detection term comes from this reference signal.

Now let us approach this process in time domain with mathematical expressions[35]. Remembering the euler's law the input signal coming from the device under test(DUT) can be expressed as follows:

$$V_s(t) = \sqrt{2}Rcos(w_s t\Theta) = \frac{R}{\sqrt{2}}e^{i(w_s t+\Theta)} + \frac{R}{\sqrt{2}}e^{-i(w_s t+\Theta)}$$

The reference signal is as follow:

$$V_r(t) = \sqrt{2}e^{-iw_r t} = \sqrt{2}cos(w_r t) - i\sqrt{2}sin(w_r t)$$

After mixing the two signals, two major harmonics which are the sum and differences of the signals.

$$Z(t) = V_s(t)V_r(t) = R[e^{i[w_r - w_s]t+\Theta} + e^{-i[w_r+w_s]t+\Theta}]$$

After the mixing, a low-pass filtering is required for signal isolation as mentioned above. Subsequent low-pass filter stages eliminates the sum frequency $(w_s + w_r)$ then we are left with:

$$Z(t) = R.e^{i[w_s - w_(t) + \Theta]}$$

If the signals are equal to each other, the last equation simplifies further to a DC component.

$$Z(t) = R.e^{i\Theta}$$

This equation contains two unknowns which are amplitude R and phase Φ therefore two equations are required to extract the independent information. The second equation comes from an almost same process but in that case the reference signal is a 90° shifted version of the former. Finally, if we take the real part of the output signal and imaginary part of the output signal coming from the shifted version of the reference signal, the magnitude and the phase of the output signal can be reached independently by manipulating the in-phase and quadrature components.

$$X = Re(Z) =< R.e^{i\Theta} >= R.cos(\Theta)$$

$$Y = Im(Z) = - < R.e^{i(\Theta + 90°)} >= R.sin(\Theta)$$

Finally, with the last two expression we can reach the amplitude and phase information as follows.

$$R = \sqrt{X^2 + Y^2}$$

$$\Theta = atan2(Y, X)$$

After getting a sufficient technical background for lock-in amplifier operation, let us explain some of the necessary practical information.

Time Constant: This value is the integration time of the low pass filter. There is always a compromise between the noise level and measurement time over time constant. The signal to noise ration (SNR) can be improved by increasing the time constant, however in that case the measurement time increases too. For setting the time constant, there is not a recipe exist, the parameters of the experiment determines it. For instance, if the experimentalist is pursuing an observation of an event whose effect will take 1ms; setting the time constant to 10ms is not a logical indeed. To obtain a reliable output signal from the LIA, the experimentalist has to wait at least five times the set time constant for low-pass filters to reach a reasonable (1%) steady state error level. As once Prof. Hanay stated: *"There is no such thing as instantaneous in experimental studies, there is always a transition."*

Dynamic Reserve: This term defines the signal extraction performance of a LIA. A good LIA on the market can have dynamic reserve up to 120dB which means that it can extract a target signal of amplitude million times smaller than the noisy background it is buried [36]. It can be confused with the term *dynamic range* which defines the interval between the thermal fluctuations and the onset of nonlinearity.

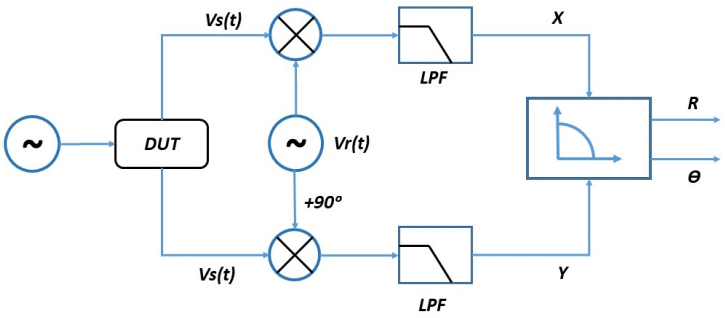

Figure 3.5: Lock-in Amplifier Operation Scheme

3.3 The Experiment Setup

The main objectives of the experiment setup are as follows:

- Drive the resonator at its first two resonant modes simultaneously.
- Downconvert the signals coming out of the resonator and read them.
- Keep the phase of the signals fixed at 0°.

Below you can examine the circuit diagram that is used for the stated tasks above. This circuit is constructed for two mode measurements. The circuit consists of microwave circuit elements power splitters/combiners (P.S. ,P.C.), rf switches (RFS), mixers, bandpass filters (BPF), lowpass filters (LPF), signal generators and a data acquisition card. The operation principles of each component are explained above, moreover, how this circuit operates with these components will be explained in detail below.

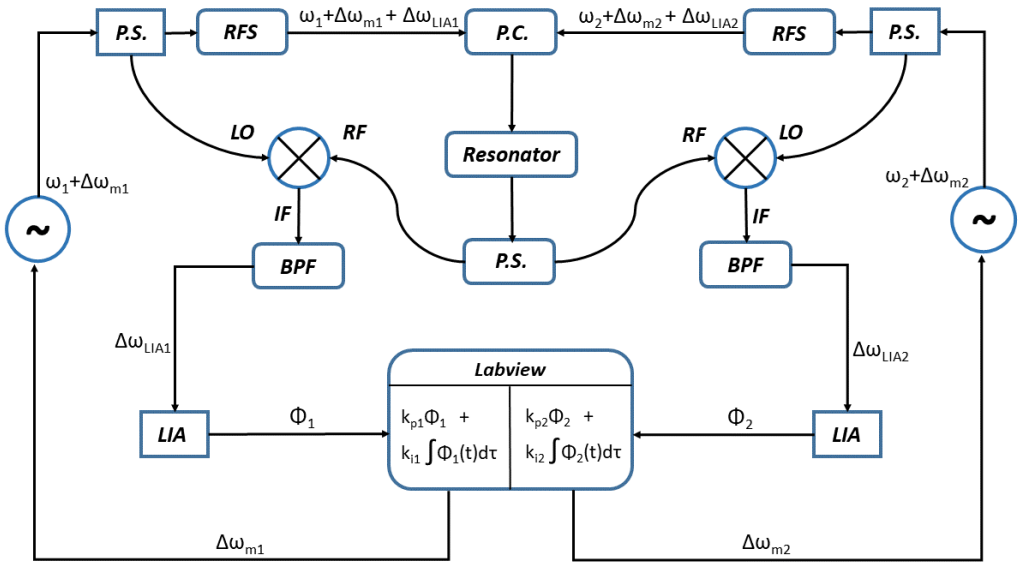

Figure 3.6: The experiment circuit

The main pumping frequencies to drive the resonators are individually and simultaneously generated by the two individual signal generators. Each main signal passes through an equal split power divider. One branch is used for frequency modulation in rf switches. The rf switch which is provided with a TTL square wave signal of frequency $\Delta\omega_{LIA1}$ is to modulate the ω_i signal. The rf switch has two rf outputs that open and close according to the supplied TTL signal provided by the LIA. One of these ports is idle and terminated with a matched load so that no reflection occurs. From the other port, the source rf signal emerges with a modulated component of $\omega_i + \Delta\omega_{LIAi}$. There are two objectives in these steps: To drive the resonator at its first two modes simultaneously and prepare the signals for downconversion. Downconversion is necessary since it is not possible to read signals on the order of gigahertz regime with LIAs. It is necessary to obtain a readable signal that carries information related to the resonator hence the signal is modulated by the rf switches. This procedure applies for both signals therefore the two modulated signals combined with a power divider just before the resonator. Later on, the $\Delta\omega_{LIAi}$ components will be extracted as information carrying signals. As a practical concern, these signals should not be of too low frequencies to avoid the $1/f$ noise.

After signals passed through the resonator another power splitting stage comes since the two modes will be read individually. The separated signals are the RF inputs of the two mixers and ready for downconversion. At this point note that RF inputs have the $\Delta\omega_{LIAi}$ components.

The other branch of the signal divided in the first stage is a pure tone sine wave, called local oscillator, is required to saturate the diode within the mixer and realize the conversion. As mentioned previously, the operation occurs within the mixer is a multiplication. The product of two signals that differ by $\Delta\omega_{LIAi}$ results in a frequency component $\Delta\omega_{LIAi}$ whereas the high frequency component is filtered out by BPF or LPF. Again as mentioned above, there are infinitely many low power harmonics exist in the spectrum hence a careful filtering stage is realized at this point.

This filtered signal is the input to the LIA. The LIA demodulates the signal to its phase and amplitude components as explained in detail above. The signal read by the LIA is sent to a data acquisition card (DAQ) connected to a computer.

Until this point, the circuit required to drive the resonators and extract the information carried signals is explained and how these signals are generated and read by the instruments are shown. In the following sections how this circuit is employed for real time measurements will be explained.

3.3.1 Characterization of the Resonators and Open Sweep Measurements

The TL resonators are first characterized with a signal analyzer or a vector network analyzer to locate the resonant modes. A spectrum analyzer can take a frequency sweep between 9kHz-3gHz(Keysight CXA, n9000a)in a very short time and read the response given to that signal by DUT at the same time so that one can obtain the frequency response of any DUT by just connecting it to the instrument. A network analyzer is used for network characterization yet it does a similar job. By measuring the S_{21} parameter which is the ratio of the reflected

wave from the second port and incident wave to the first port one can locate the resonant frequencies where S_{21} parameter have maxima. This initial characterization of the TL resonators solely for obtaining an idea about the location of the resonant modes.

Following that another open sweep which takes place to locate the zero phase crossings. Here, signal generators produce signals in the given frequency range with predetermined step sizes on labview environment. For example, the loci of the resonant frequencies are known thanks to the previous characterization, following that a sweep of 200 MHz around the resonant frequencies are taken individually. This is because the resonator is driven at a frequency in the close vicinity of resonant frequency where the output signal carries 0° phase. In the close loop measurement section we will return to this discussion. Below you can examine the circuit required for open loop measurement.

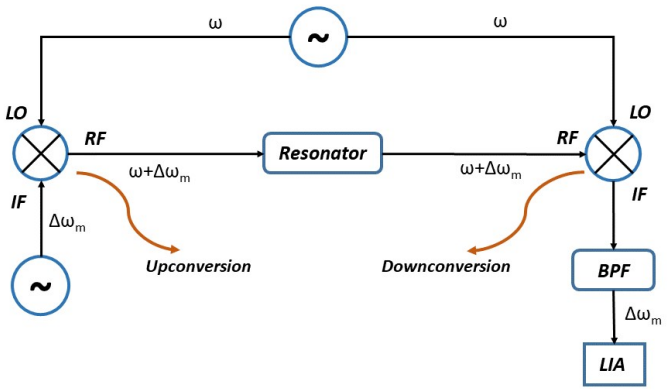

Figure 3.7: Open Loop Frequency Sweep Scheme

As aforementioned in the mixer section, upconversion and downconversion are frequently employed procedures in our experiment setup. Notice how the mixers are used in this circuit. In the left hand side of the circuit, the reference output of the LIA is sent as an input to the IF input of the mixer. This frequency is tied to the internal oscillator of the LIA which means that LIA will look for the component of the same frequency while signal detection. First it is upconverted to levels on the order of gHz by the local oscillator signal supplied from the signal

generated then passes through the resonator as the response of the resonator. Since the used resonator is a linear model the superposition and time invariance properties are valid therefore resonator gives a response at the same frequency with a modulated amplitude and a phase delay. The figure can remind the reader how linear time invariant (LTI) systems behaves.

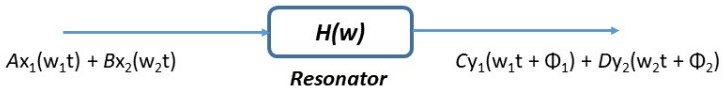

Figure 3.8: A depiction of superposition and time invariance in a linear model

On the right handside of the circuit the information carrying upconverted signal is ready to be downconverted. This time RF port of the mixer is used an input and IF is the output of the mixer. Again, the LO port of the mixer is fed through the signal generator with a strong signal according to the level of the device. The information carrying signal which has a frequency slightly above than the frequency of LO signal can be converted in the mixer. After multiplication stage an LPF/BPF is planted to eliminate the higher frequency components and the signal is ready to be read in LIA. The read signal is the frequency response of the resonator hence the open loop sweep concludes its operation.

3.4 Setting up the Data Acquisition

Up to this section it is explained how the resonator is driven, the circuit required to obtain the information carrying signal and the read out scheme is constructed.

The signal reading process is realized within the LIA however those data needs to be available in the computer environment for further manipulation. LIA can generate the signal it reads and generate that signal as its auxilary output. Indeed, the auxilary output is an analog signal yet a digital signal is needed for transmitting the signal to computer environment. (This requirement was also needed to accomplish open loop sweep). At this moment an analog to digital converter data acquisition card (DAQ) is employed. The model is National Instruments .... Through this card the read signals can be used as input within the written labview codes and it is possible to conduct real time experiments.

3.5 Phase Locked Loop(PLL) Control Scheme

The most critical part of the experimental setup is the software based control scheme. The control scheme operates with the designed circuit in harmony and allow the experimentalist to conduct real time sensing operations. In aforementioned sections it is mentioned that the resonator is driven at a frequency in the close vicinity of the resonant frequencies where the phase of the response is 0°. If we just find this frequency and send it continuously it is not possible to conduct an experiment because that frequency is volatile due to vibrations in the environment, thermal fluctuations due to currents flow through the resonators, the electromagnetic interference engendered by the waves bounce back from the laboratory environment and so on. Therefore after locating the zero phase condition it has to be kept that way. Another main purpose in doing so is the microfluidic experiment's nature itself. When a cell or droplet comes under the sensing region of the resonator because of the permittivity modulation the resonance frequency shifts to some other frequency, thus the zero phase frequency. The close loop control scheme, which is called phase locked loop (PLL), ensures that the output is fixed at zero phase means that the control scheme is continuously trying to lock in zero phase as the name suggests. According to this, if a target particle shifts the resonant frequency with its presence, PLL locates the zero phase frequency and the difference between the frequency before the particle and after is the frequency shift that we use in our calculations. Besides the shifts coming from the

particle presence, PLL also eliminates the phase shifts of the agents mentioned above.

The designed PLL is comprised of a proportional K_p and an integrator term K_i therefore it is classified as a PI controller. The input of our PLL design is frequency whereas the output is the phase of the measured signal. One noteworthy aspect of this control scheme is that the transfer function of the resonator is not necessary. Since the experimentalist knows the frequency supplied from the signal generator at all times and can demodulate and measure the response of the resonator perpetually the implementation of the controller in the labview environment is simple.

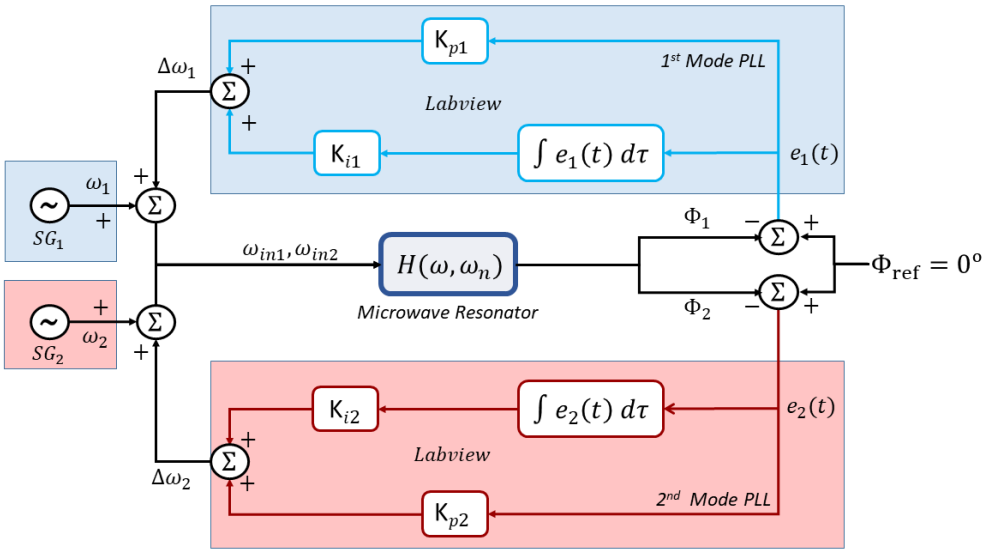

Figure 3.9: Interplay of control scheme embeddedi in labview with microwave circuitry

In the labview code, the error term is defined as the phase of the signal. So long as the phase is not zero the frequency written in the signal generators are updated according to the output of the proportional and integrator terms. If the phase is fluctuating around 0° there will not be a drastic change in the main frequency that drives the resonator. However if there is significant phase then a significant

frequency change follows it. If the experimentalist is continuously measuring high phase values despite the controller is updating the main frequency indicates that the resonant frequency is shifted some other location beyond the vicinity of the resonant freqeuency. If this is the case then another open loop measurement must be taken. If the phase changes suddenly which is the case during the experiments the control loop updates frequencies pretty fast and relocates the 0° condition.

3.5.1 Labview Implementation

In the previous section the control scheme is explained. The interplay between the designed circuit and PLL occurs within the labview code. The equipment used in the experiments are defined as objects used for writing and reading purposes. In the aforementioned section it is stated that the error term is the read phase value. It is also also stated that the demodulation of the signal occurs within the lock-in amplifier. The lock-in amplifier is capable of generating the signal it demodulates as phase and magnitude values from its output ports. On the software options two of the output ports are chose to take out the phase and magnitude values as an AC voltage. This analog AC voltage has to be converted into digital and supplied to the computer environment. At this point a DAC card is connected to computer and two of its input ports defined as voltage inputs. This definition is realized within the labview environment. As a result, when the input ports are defined as voltage input objects the demodulated signal outputs of LIA is defined as objects in labview environment for reading purposes. This procedure is repeated for two modes, indeed for two LIAs which constructs the reading section of the code.

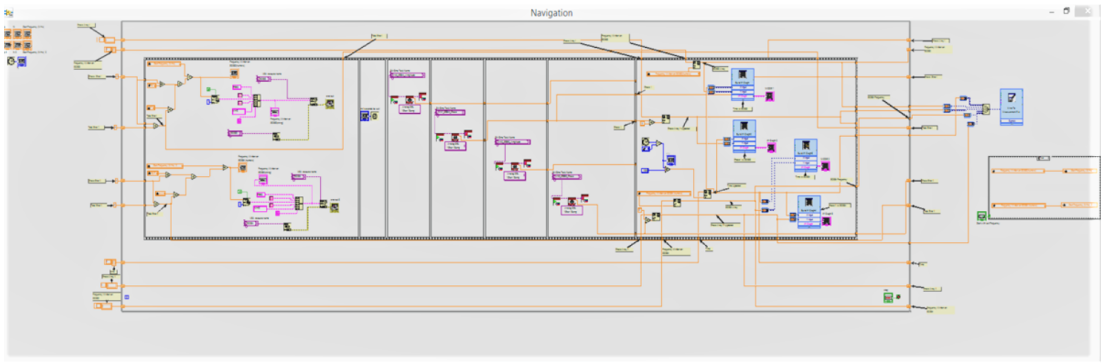

Figure 3.10: Labview code to read the signals on computer environment and update the frequency written on signal generators for two modes

The read values are the error terms $e_1(t)$ and $e_2(t)$ which are the argument of the feedback controller. According to the output of the controller the signals $\Delta\omega_1$ and $\Delta\omega_2$ terms are generated. These are the values to be added on the main driving frequencies ω_1 and ω_2 so that the zero phase can be tracked. To add these signals, the signal generators needs to be defined as objects and writing operation on these objects are realized in labview environment. The connection between the signal generators and the computer is realized through LAN connection with an ethernet cable. The generated frequency output terms are written to the signal generator objects as addition.

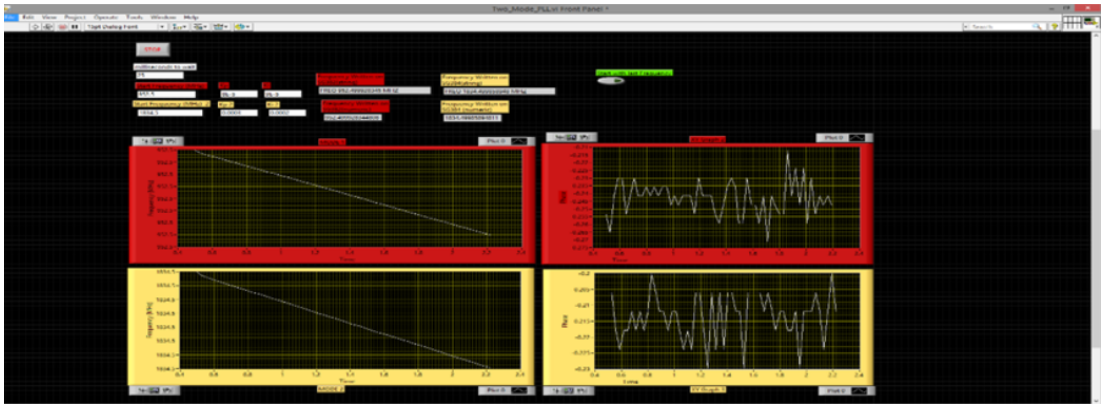

Figure 3.11: The interface created to make the operation user friendly

Remark: The LAN connection procedure is faster and more compact compared to GPIB connection procedure. Besides, since IE-488 cables are not needed, the LAN connection realized with ethernet cables is cheaper.

3.6 Sensitivity & Resolution

In the aforementioned sections it is mentioned that the dynamic range of the NEMS resonators are sandwiched between the omnipresent thermal fluctuations and onset of nonlinearity for the specific device and the employed measurement scheme. The resolution of the resonators merged with our measurement circuit is quantified by the allan deviation and limited by the frequency fluctuations[37], [38],[39].

During the microdroplet experiments, -indeed in correlation with the chosen control parameters- the allan deviation is calculated to be 5.10^{-7} for both modes at the response time. For a resonator which is operated at $1.4GHz$ this value means that the intrinsic frequency fluctuation is $0.7kHz$ for a response time approximately 500ms. Consequently, if a microdroplet passes through the channels and creates a frequency shift less than $0.7kHz$ it can not be detected by the resonator since there will not be a meaningful and comfirmable frequency shift. In the conducted microdroplet experiments, according to the position, the events generated a frequency shift not less than $30kHz$ thus the events are characterized with clarity.

As for the cell experiments same devices are operated, yet different control parameters are chosen to tailor the control scheme for the cell events which create a subtle frequency shifts compared to microdroplet events. This is because the smaller volume of the cells. The allan deviation value for the cell experiments are calculated to be 2.10^{-8} for both modes and the resonant frequencies of the devices are at the same loci. Hence the detectable minimum frequency shift for a cell event in this case comes up to be $29Hz$. Consequently if an event creates a frequency shift larger than this quantified fluctuation level it can be used in our

calculations for information extraction. The smallest frequency shifts are caused by HeLa cells -since they are smaller than MDA-MB-157 cells- yet they are not less than $1kHz$ that enables the experimentalist to classify the shifts as events.

Chapter 4

Results and Discussion

After getting promising results from the simulation and first generation pipetting analyte experiments and with the measurement circuit and control scheme established, it is possible to conduct real time experiments. Again at this stage the researches followed a gradual paradigm by starting these experiments with large flowing analytes such as generated water droplets in oil as conducting liquid. After ensuring that the location and electrical volume of the droplets are calculated via frequency shifts and higher order mode shapes, the researches moved on to measure smaller particles such as cervical (HeLa) and breast cancer (MDA-MB-157) cells. In this section the results regarding these experiments will be shared and impact of our application will be discussed.

4.1 Manufacturing of the Resonators with Microchannel

To realize the research aim of sensing analytes in real time, a microfluidic channel embedded resonator is needed. The fabrication of the device is as follows. First, a mask that carries the microfluidic channel features is produced. The mask is drawn and manufactured with electron beam lithography. A high resolution

in mask manufacturing is required since the resolution of photolithography is limited with $10\mu m$. Then, a silicon wafer is covered with negative photoresist SU-8 on the top surface. The covered wafer is processed in photolithography with the produced mask that permits light only in the desired features. After photolithography the covered wafer is dipped into a developer which dissolves the parts of SU-8 that do not exposed to light. Since at this step the features of the channel is obtained, polydimethylsiloxane (PDMS) is poured on the features to transfer the pattern onto this substrate. Following the pouring stage, PDMS is degassed so that it fits the features without bubbles in it. Then the degassed PDMS wafer couple is baked and then solidified yet soft PDMS substrate is removed from the wafer with channel features. Simultaneously a copper plate which will become the ground plane of the resonator is covered with PDMS to be bonded with the previous processed part. As final step, a thin -almost 2D- copper line is bonded on top middle of the structure to form the signal line. Following the assembly of the SMA connectors for microwave signal connection, the resonator is ready for experiments. Below in the figure reader can examine the fabrication flow of the structure.

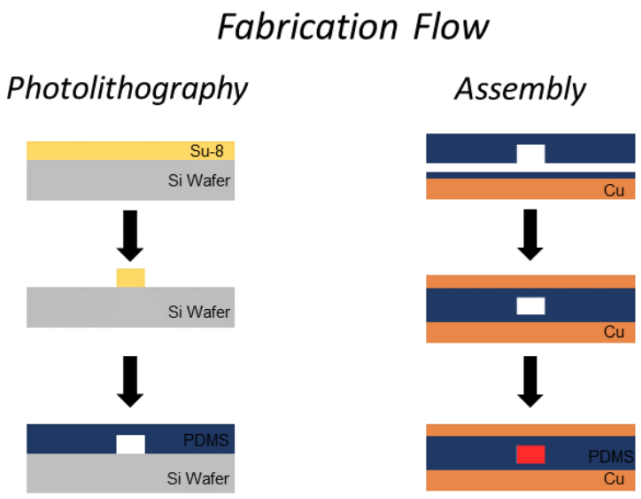

Figure 4.1: Fabrication flow of the microwave resonators containing microfluidic channels

As mentioned in the fabrication flow explained and depicted above, in the

figure below the silicon wafer that hosts microfluidic channel features can be examined. Notice that the shown device contains the same features in figure 4.2.

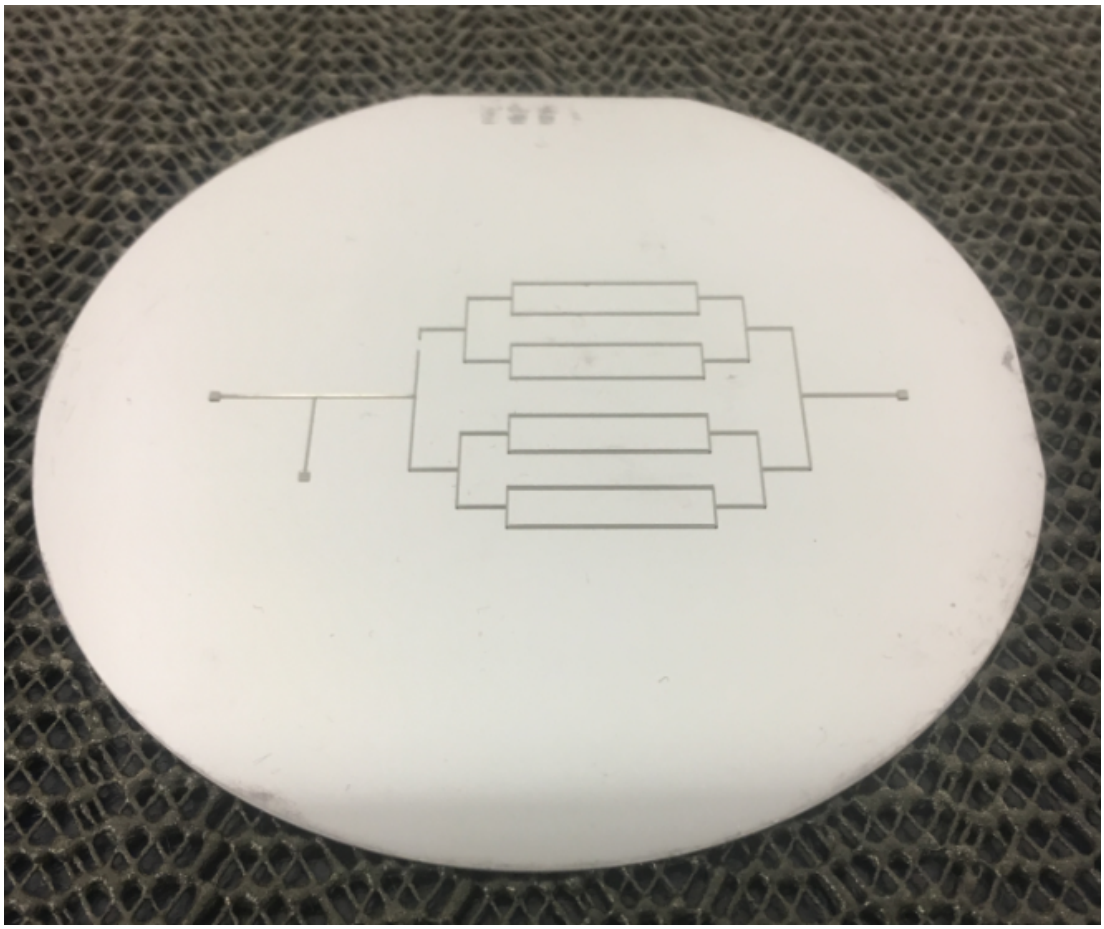

Figure 4.2: The silicon wafer mask after photolithography to transfer the features to PDMS substrate

Below, the resonator that is used in the experiments is shown. The 2 ports on the right are for the carrier fluid and the droplets. From one port oil is continuously pumped and from the one in the near vicinity, the generated droplets are sent. The leftmost and let alone port is the exit port. The channel feature is designed as four branches for testing purposes. In this way it is possible to track the trajectories of the droplets or cells by allowing them to choose the part almost randomly. Only one half of the resonator is used as sensing region, therefore four branches left idle, nonetheless there are eight branches in the structure to retain

the symmetry and mode shapes in the structures as much as possible. Ink mixed water is sent through the channel to show the channels with clarity.

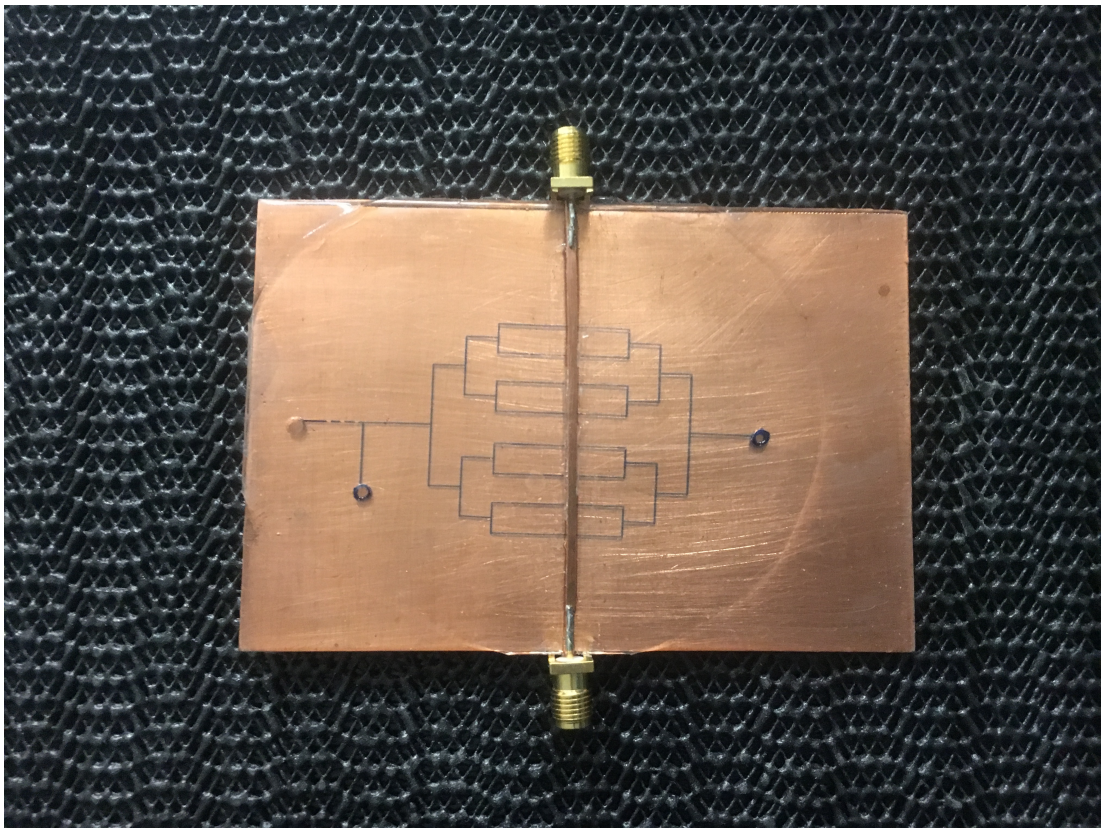

Figure 4.3: Microfluidic channel embedded microwave TL resonator

4.2 Real Time Droplet Experiments

The first real time measurements are run to detect the position and electrical volume of water droplets. To increase the permittivity contrast, oil $\epsilon_{oil} = 2.5$ is chosen as the carrier fluid whereas the generated droplets are of water $\epsilon_{water} = 78.5$. Oil is continuously pumped with high precision micro-pumps from one port and via the other port the water droplets are sent by hand. The generation and path of the water droplets are followed with a sterio-microscope on computer environment to confirm the measured frequency shifts are engendered by passage events. Since the hydraulic resistance of the microfluidic channel branches are

almost identical, the generated droplets choose their path in an almost random fashion.

Before sending the droplets, the resonator is already being driven by the two mode measurement circuit and PLL. Therefore if an event(passing of an analyte under the sensing region through the branches) they cause a frequency shift and it is recorded in real time. The obtained raw data proves the fact that the frequency shifts occurs according to the electric field intensity. The loci of the microfluidic channels arranged so that at first lateral channel the magnitude of the first mode is larger, at second position two modes have almost the same intensity, at third position second mode has higher magnitude whereas at fourth position the second mode has a node hence although a passage event occurs it does not beget a frequency shift in second mode PLL. Below the reader can examine the obtained data from one of the droplet experiments.

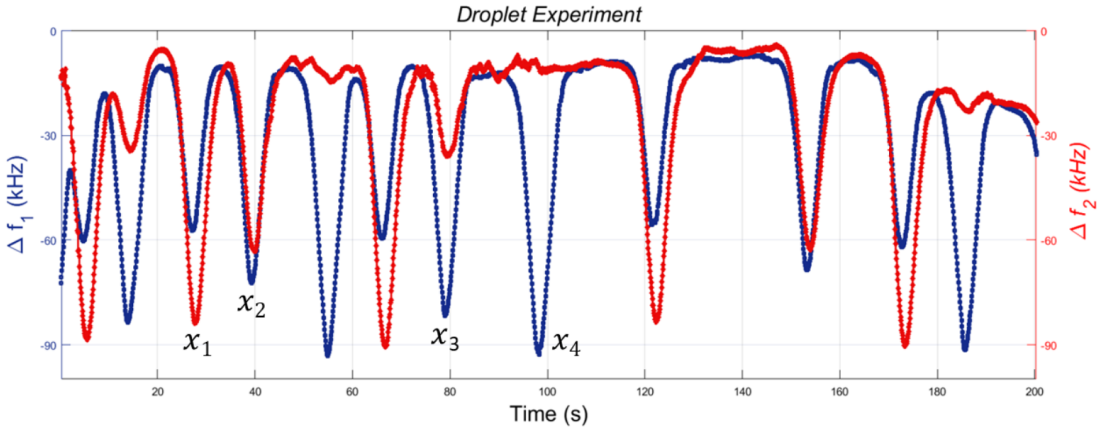

Figure 4.4: Frequency shifts due to the droplet passages

It can be seen that because four branches of microchannels located at normalized positions of $x_1 = 0.31$, $x_2 = 0.37$, $x_3 = 0.44$ and $x_4 = 0.5$ the occurred frequency shifts differ in amplitude. Frequency shifts occurs with respect to the intensity of electrical field of the mode shape which is position dependent can be seen in the depiction below.

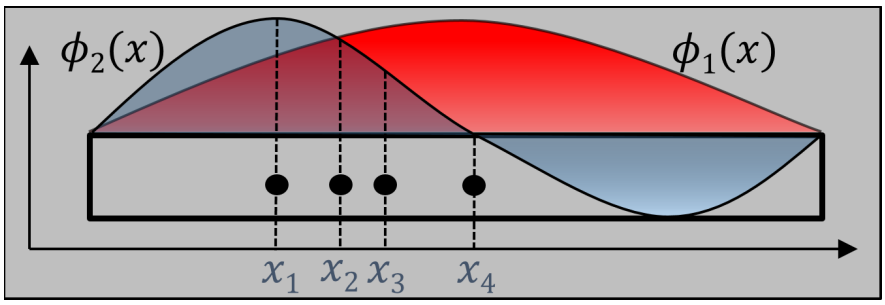

Figure 4.5: Position dependent frequency shifts due to mode shapes

According to this, when a droplet passes through the location x_1 the shift in the second mode is greater than the second whereas it passes through x_4 almost no shift occurs in second mode since it has its node there. At location x_2 the magnitude of the two modes are in close proximity therefore the frequency shifts are almost identical and at location x_3 the shift occurred in the first mode exceeds the second one just because of the same reason.

The frequency shifts amassed during multiple numbers of experiments are drawn on $\delta f_1 - \delta f_2$ plane. When a $\delta f_1 - \delta f_2$ frequency shift plane is generated and locate the frequency shift caused by an individual particle on this plane, it can be seen that each specific position on the sensing region of the resonator fall in to a unique line with a certain incline. So, no matter the type and volume of the particle, if it passes through the location x_i, the frequency shifts caused by that particle will be on a specific line that can be seen in the figure below.

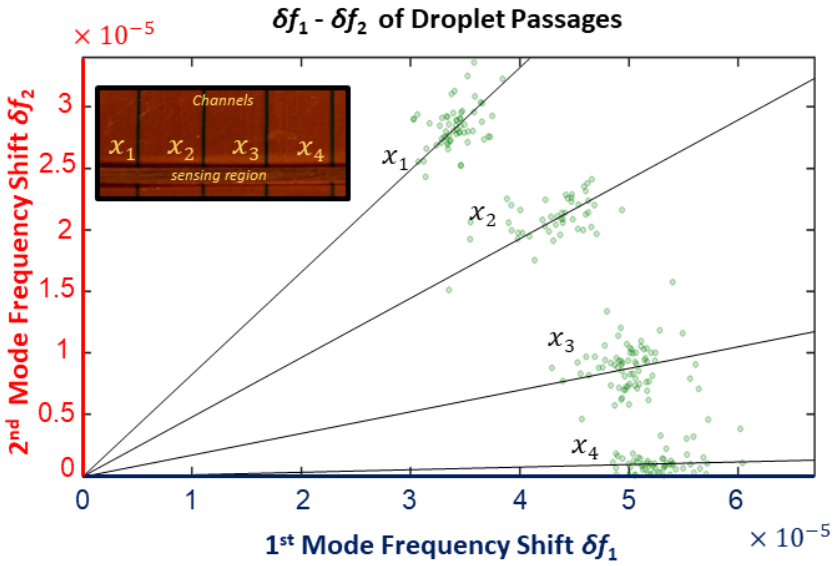

Figure 4.6: Position dependent frequency shifts on $\delta f_1 - \delta f_2$ plane. Reprinted with permission of Royal Society of Chemistry, Lab on a Chip Journal, Issue 3, 2018.

Once the frequency shift induced by a signal droplet is recorded, its position information can be calculated by the theory elaborated in section 1. The data points presented in figure 4.6 are exploited to calculate the position of the droplets and represented in the histogram below. The histogram supports the statement that the droplets chose their channel branch in an almost random manner.

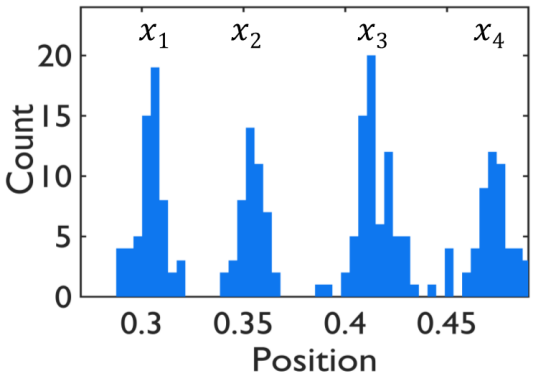

Figure 4.7: Calculated positions of the droplets. Reprinted with permission of Royal Society of Chemistry, Lab on a Chip Journal, Issue 3, 2018.

Once the position of a single droplet is calculated from the frequency shift it induced in the first two modes the electrical volume can also be calculated from either of the equations 1.24 and 1.25. Regarding this fact the electrical volume information of the individual droplets are calculated and drawn in the histogram below.

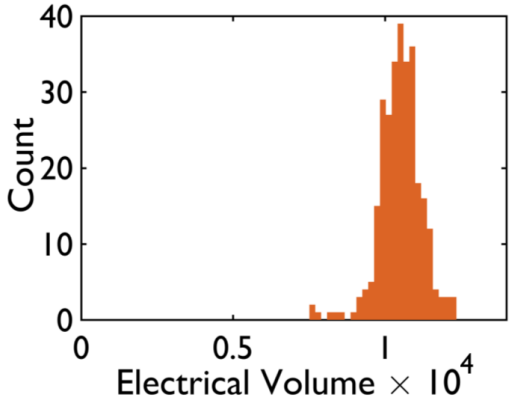

Figure 4.8: Calculated positions of the droplets. The center of the histogram corresponds to a volume of water that is $\approx 60\mu m$ in diameter. Reprinted with permission of Royal Society of Chemistry, Lab on a Chip Journal, Issue 3, 2018.

4.3 Real Time Cell Experiments

Once the real time droplet experiments are conducted successfully by achieving the aim to detect the position and electrical volume information by manipulating the experimentally obtained frequency shifts and using the theoretical mode shapes of the structure, the researchers move forward in the pursuit of smaller particles; cells.

The experiments are conducted on the same resonator structure with the same size as it was in the droplet experiments. This time the requirement for two fluidic ports are not necessary since the analytes are not generated. Usage of one port to send the liquid medium that carries a certain concentration of cells are sent and the leftmost port is for evacuation. During the experiments the sedimentation of cells to the bottom occur therefore after a certain number of experiment runs, the cell container is needed to be shaken.

The experimental procedure is also same as it was in the droplet experiments. The cells are contained in a culture medium stocked in a syringe is sent through the fluidic port of the device with a certain volumetric flow rate adjustable on a syringe pump. The only single difference between the droplet and cell experiments is that the droplets chose their fluidic path in almost randomly as it can be seen in the position histogram, figure 4.7. However, due to the intrinsic feature discrepancies between the channels originates from the manufacturing and bonding uncertainties and unequal PDMS thickness the cells chose the least resistant fluidic path. This was not the case for the droplets since the hydraulic pressure difference between the paths are not significant for analytes for their volume.

The experiments are repeated for many times with different volumetric flow rates for two kinds of cell lines. The first cell experiments are based on HeLa (cervical cancer) and the second one is based on MDA-MB-157 (breast cancer). The raw data of frequency shifts due to the presence of cells that pass under the sensing region can be examined below for both types of cells.

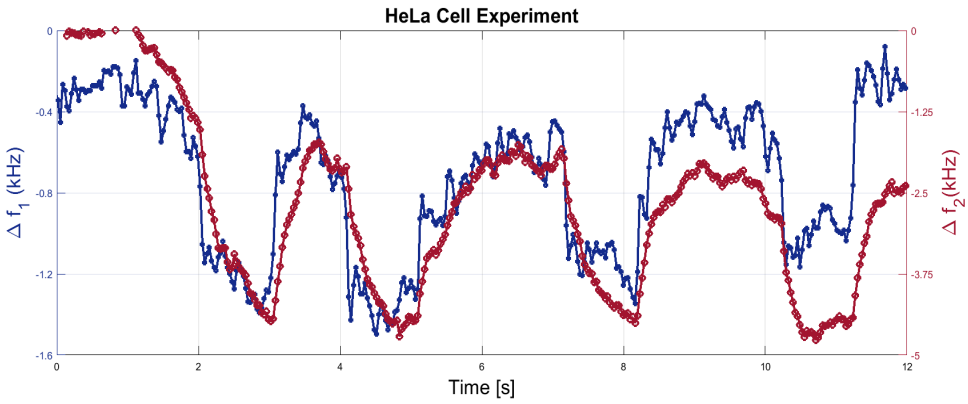

(a) Frequency shifts caused by HeLa cell passages

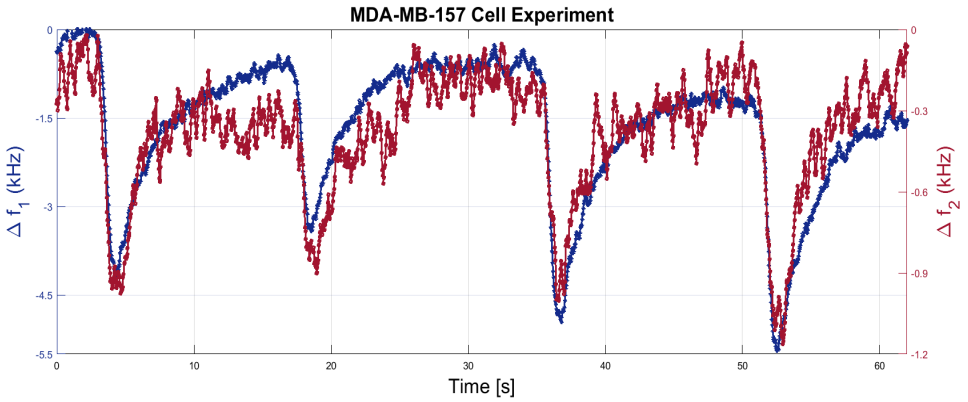

(b) Frequency shifts caused by MDA-MB-157 cell passages

Figure 4.9: Raw data from cell experiments

Regarding the stated reason above, the position calculations are not shown since all the cells passed through a single channel. From data recorded in the experiments, the electrical volume calculation of the individual cell are realized. MDA-MB-157 cells are larger than HeLa cells and our calculation supports this fact. The calculations belong the electrical volume of the HeLa cells are measured to be 15.2 x 10^{-7} with a standard deviation $\sigma = 5.8$ x 10^{-7} as for the MDA-MB-157 cell line the mean of electrical volume comes up to be 3.93 x 10^{-6} with a standard deviation $\sigma = 8.4$ x 10^{-7}. The results indicate the size of MDA-MB-157 cells are larger in volume where this fact is supported by the histogram provided below.

Remark: Notice the monodispersed size population of each type of cells.

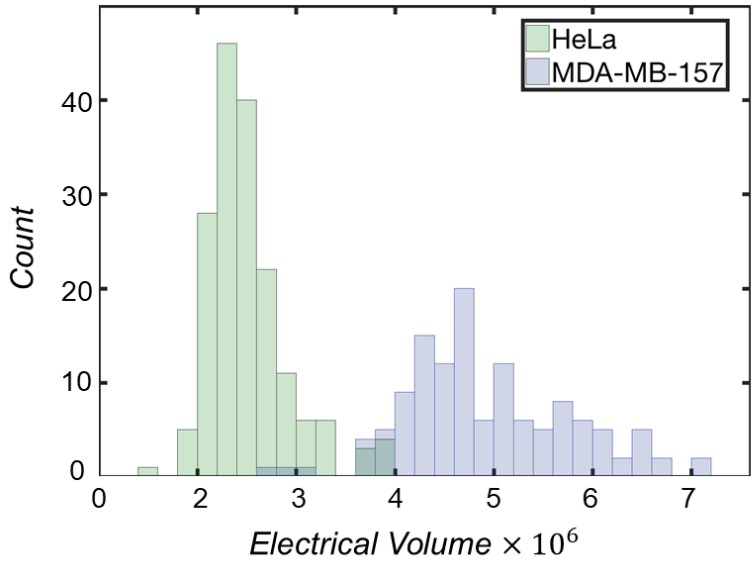

Figure 4.10: Calculated electrical volume of the cell lines HeLa and MDA-MB-157 during the experiments.Reprinted with permission of Royal Society of Chemistry, Lab on a Chip Journal, Issue 3, 2018.

4.4 Future Developments

Microstrip TL resonators are good candidates for 1D resonator applications and emulate the success of NEMS resonators in electromagnetic domain. However, the pursuit of higher Q resonators are necessary to increase the resolution and sensing pace of the resonators. The split ring resonators have a reputation of being high Q structures [40]. Their intrinsic mode-shapes without forcing any boundary conditions are shown to be appropriate for high-order mode sensing theory. After a careful examination of the structure in terms of electric field distribution, the loci for micrfluidic channel implementation and resonant frequency loci versus geometric size, ring resonators can be exploited as next generation two-mode sensing structures with higher performance.

According to specific purposes of position detection of organelles or high throughput analyte counting with high SNR levels, a better resolution is a must. To increase the SNR levels and ameliorate the resolution, the induced frequency shifts by the analytes should be much larger than the fluctuation level. A viable solution to this necessity is tapered resonator structures, such as tapered coplanar waveguides. Since the electric field intensifies at the tapered location, the particle presence induces larger frequency shifts compared to the straight line resonators. A mask is created in matlab environment to be transferred to Clewin for manufacturing is designed. In this design the tapered geometry is adjusted so that at any differential length the characteristic impedance is 80 Ω. This structure can be further studied for its adaptation to cell sensing applications. Below the drawn top copper plane of the structure can be examined.

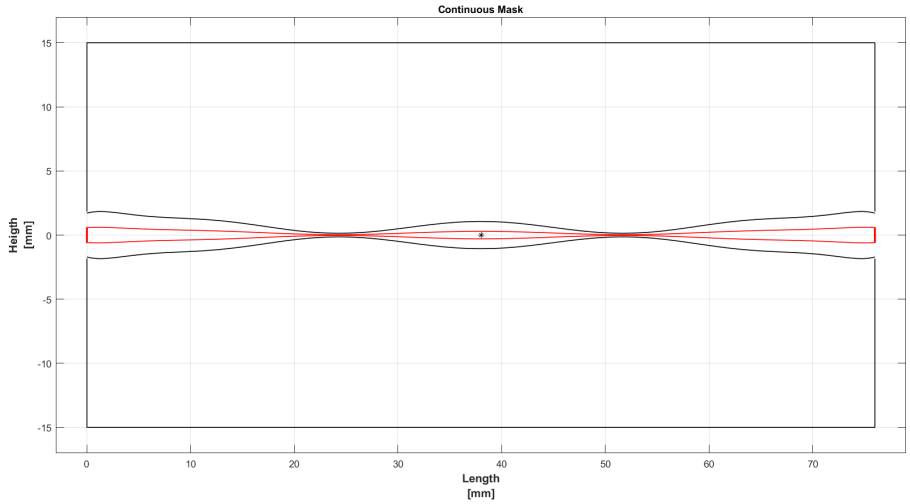

Figure 4.11: Tapered CPW structure for cell sensing applications

The material search and optimum geometrical features for TL resonators to maximize the performance is an ongoing pursuit in this research. The materials that would yield lower dielectric loss while having the characteristic of biocompatibility and that would reduce the size of the structure is an optimization problem [41]. The volumetric ratio of the structure and the cell is an important parameter contributes to the signal to noise ratio. If the resonators can be made smaller in length and width, the volume of the analyte becomes more significant

compared to the volume of the resonator. Therefore it is possible to reach higher sensitivity values with better SNR levels. Besides, this ratio can be improved by thinning the signal line. In the end, the effective resonator volume is defined as volume under the signal line. By making simulations focused on these particular perspectives, manufacturing new resonators and conducting experiments with them a significant experience can be amassed that would be beneficial in next stages of the research.

The scope of this thesis is limited with the two-mode microwave sensing. Yet, the necessary measurement circuit to accomplish seven-mode measurements are also studied. Below the microwave circuit based on rf switch frequency modulation for seven-mode measurement is designed.

Remark: The necessary filtering steps while separating the modes from each other are omitted for clarity. The terms P.C. stands for power combiner whereas P.S. for power splitter. Since this device is symmetrical and bidirectional the terms are interchangable hence they refer to a single type of device.

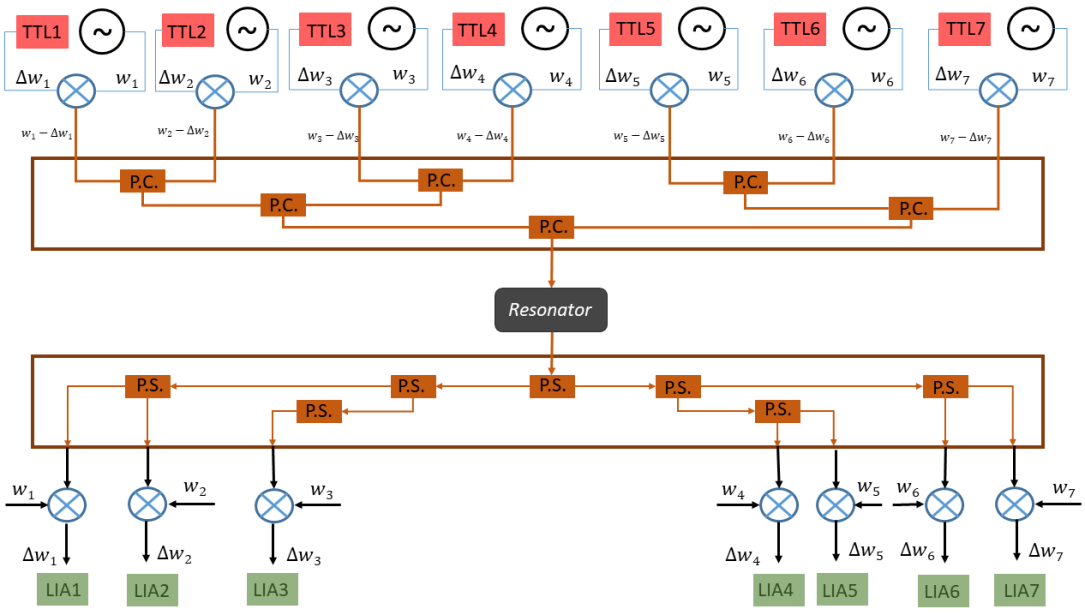

Figure 4.12: Microwave circuit for seven-mode measurement

The sensing system we proposed in this research can be branched into many

other measurement schemes. The main operating principle of this resonator based application is built on the fact that effective permittivity change modulates the resonance frequency of the device. Therefore, the method we propose here can be used for gas chromatography, pulse sensing, pressure and temperature measurement for both liquids and gases so long as the permittivity is mathematically expressed as a function of frequency with clarity and building a high precision minute proximity/motion sensor.

4.5 Discussion & Conclusion

With the proposed microwave resonator based sensors, measurement of location and electrical volume of analytes ranging from microdroplets to individual cells are demonstrated. A novel analogy is established between the mechanical and the electromagnetic domains to extend the usage of higher-order mode theory for real time particle sensing from NEMS resonators to their electromagnetic counterparts: microwave resonators.

The main motivation behind these endeavors is that both doubly-clamped beams and microwave TL resonators can be tailored to have the exact same mode shapes for the nth resonant mode expressed as $\Phi_n = sin(pinx)$ where x is the spatial coordinate. In the case of doubly clamped beams, the supporting points are stagnant so that at resonance the pure sine shapes can be reached. As for the microwave resonators the boundary conditions are defined as shorts so that the voltage value at these points are just 0. In this way at resonance, a voltage profile in pure sinusoidal shape can be reached. Both resonators can be exploited as 1D resonators with benign approximations that do not deteriorate the certainty of calculations.

In mechanical domain the sensing task is realized by inducing frequency shifts due to the adhesion of particles on the beam surface. It is shown that the same task can be accomplished when the effective permittivity of the resonator is modulated by the presence of a particle within the sensing region where electric field

has sufficient intensity.

The analogies between the higher-mode sensing theory's mechanical and electromagnetic application are shown. For both domains, the main information extraction parameter is the induced frequency shifts. Moreover, for both domains the mathematical expression of the frequency shifts derives from the energy equations before and in the course of sensing. After all, in mechanical domain the resonant phenomenon is based on a certain deformation scheme with maximum amplitude, thus the energy equations are based on kinetic energy. Whereas the resonance phenomenon in the electromagnetic domain is based on standing wave patterns generated by reflected and incident electromagnetic waves, the main terms of the energy equations are electric and magnetic fields.

With all these conspicuous aspects of similarities between two domains, extending the higher-order mode sensing theory into electromagnetic domain is able to be realized. The endeavors dedicated to this purpose started with finite elements simulations. Then first generation non-real time experiments are realized as an initial step into the reality. Starting from larger analytes such as pipetted droplets and microdroplets then moving to the tiny particles such as cervical and breast cancer cells, the capabilities of the proposed theory, the measurement circuit and the manufactured microfluidic channel embedded microwave resonators are demonstrated with success.

One of the significant aspects of the proposed sensing method is that for the sensing operation to be realized a close proximity of particles is not a necessity as it is in the capacitance based sensors[42]. After stating the fact that the fringing fields have negligible magnitude compared to the field between the conducting surfaces, the whole volume beneath the signal line can be exploited as sensing region. In fact, this aspect bestows the ability of making position dependent measurements to the structure. As it is represented by the data obtained from the experiments, the nearly same sized droplets induce different frequency shifts since the mode shapes -hence the intensity of electric field- varies along the structure. Besides, the presence of a particle modulates the effective permittivity of the whole structure, therefore the mode-shapes become tools to extract this

modulation as information.

The main purpose of this study is to produce an affordable, table top and fully electronical alternative to the bulky and expensive optical microscopy methods. The two mode sensing is the beginning to the final destination. By employing 3D resonators such as cavities where the standing wave patterns are formed in all directions and by using higher-order modes such as the first fifteen modes, it is possible to calculate the higher order moments of the change of permittivity distribution function $\Delta\epsilon(r)$ belongs to the volume of particle. As it is explained in the aforementioned sections in every moment there is a specific piece of information is embedded. For instance by the first moment the location and electrical volume of the particle, the second moment the extent of the particle which defined as the dispersion of particle volume around its mean position and by higher order moments the size, orientation, height and permittivity of the particle can be obtained. Ultimately the next generations of this application will end up in a novel, on table, affordable and non-contact imaging product that operates in microwave regime.

The operation in microwave regime provides certain advantages that are missing in optical counterparts. One of the most striking aspect of these advantages is the contrast. For example, in optical imaging the refractive index of the biological medium that hosts the cells and the refractive index of cells are close to each other which requires a precise focusing for a high quality image. However as for the microwave domain, the difference between the permittivities of the medium and the cells -i.e. $\epsilon_{water} \approx 76$,$\epsilon_{cell} \approx 4$ - are much larger. This intrinsic property of the domain allows to obtain image with much ease. The inherent permittivity contrast reduces the computational power required to extract information from intensely pixelated image in optical imaging applications.

Another striking aspect of microwave imaging compared to optical ones is its being non-contact. In optical imaging systems the sample to be examined is squeezed between two glass slides. Attributable to the imposed pressure on the sample, the cells may change their volumes therefore the obtained image is a distorted version of the reality. Thanks to the non-contact measurement scheme,

the microwave imaging product has the ability to excel the optical systems. Besides, being non-contact also makes the imaging scheme non-invasive, reduces the requirement of extra tools and processes such as glass slides, plastic gloves and sample preparation.

The proposed microwave imaging technique promises to obtain information related to both morphological and electrical properties of the analytes simultaneously. Since cancer cells or cells transforming into cancer cells have different morphological and dielectric properties than the normal ones, this aspect provides a larger set of indicators that can be beneficial in cancer detection application.

Even merely exploiting a single mode measurement it is viable to track the trajectory of a moving particle which can be exploited to produce a cell counter system. With our two-mode measurement technique, we showed that it is possible to discriminate cells from different lines, measure the electrical volume of individual cells, count the analytes that pass through multiple number of channels, observe cell growth rates and make indirect deductions pertaining to life phases of a single cell.

Bibliography

[1] M. Roukes, "Nanoelectromechanical systems face the future," *Physics World*, vol. 14, no. 2, p. 25, 2001.

[2] H. G. Craighead, "Nanoelectromechanical systems," *Science*, vol. 290, no. 5496, pp. 1532–1535, 2000.

[3] A. K. Naik, M. Hanay, W. Hiebert, X. Feng, and M. L. Roukes, "Towards single-molecule nanomechanical mass spectrometry," *Nature nanotechnology*, vol. 4, no. 7, p. 445, 2009.

[4] K. Ekinci, X. Huang, and M. Roukes, "Ultrasensitive nanoelectromechanical mass detection," *Applied Physics Letters*, vol. 84, no. 22, pp. 4469–4471, 2004.

[5] K. Jensen, K. Kim, and A. Zettl, "An atomic-resolution nanomechanical mass sensor," *Nature nanotechnology*, vol. 3, no. 9, p. 533, 2008.

[6] T. P. Burg, M. Godin, S. M. Knudsen, W. Shen, G. Carlson, J. S. Foster, K. Babcock, and S. R. Manalis, "Weighing of biomolecules, single cells and single nanoparticles in fluid," *nature*, vol. 446, no. 7139, p. 1066, 2007.

[7] A. Bogner, C. Steiner, S. Walter, J. Kita, G. Hagen, and R. Moos, "Planar microstrip ring resonators for microwave-based gas sensing: Design aspects and initial transducers for humidity and ammonia sensing," *Sensors*, vol. 17, no. 10, p. 2422, 2017.

[8] S. Majidifar and G. Karimi, "New approach for dielectric constant detection using a microstrip sensor," *Measurement*, vol. 93, pp. 310–314, 2016.

[9] G. Gennarelli, S. Romeo, M. R. Scarfi, and F. Soldovieri, "A microwave resonant sensor for concentration measurements of liquid solutions," *IEEE Sensors Journal*, vol. 13, no. 5, pp. 1857–1864, 2013.

[10] M. Ateeq, A. Shaw, L. Wang, and P. Dickson, "An innovative microwave cavity sensor for non-destructive characterisation of polymers," *Sensors and Actuators A: Physical*, vol. 251, pp. 156–166, 2016.

[11] J. Goh, A. Mason, A. Al-Shamma'a, S. Wylie, M. Field, and P. Browning, "Lactate detection using a microwave cavity sensor for biomedical applications," in *Sensing Technology (ICST), 2011 Fifth International Conference on*, pp. 436–441, IEEE, 2011.

[12] S. Stuchly and C. Bassey, "Microwave coplanar sensors for dielectric measurements," *Measurement Science and Technology*, vol. 9, no. 8, p. 1324, 1998.

[13] A. Ebrahimi, W. Withayachumnankul, S. F. Al-Sarawi, and D. Abbott, "Microwave microfluidic sensor for determination of glucose concentration in water," in *Microwave Symposium (MMS), 2015 IEEE 15th Mediterranean*, pp. 1–3, IEEE, 2015.

[14] M. H. Zarifi and M. Daneshmand, "Non-contact liquid sensing using high resolution microwave microstrip resonator," in *IEEE MTT-S Int. Microw. Symp. Dig.*, pp. 1–4, 2015.

[15] T. Chretiennot, D. Dubuc, and K. Grenier, "A microwave and microfluidic planar resonator for efficient and accurate complex permittivity characterization of aqueous solutions," *IEEE Transactions on Microwave Theory and Techniques*, vol. 61, no. 2, pp. 972–978, 2013.

[16] A. A. Abduljabar, D. J. Rowe, A. Porch, and D. A. Barrow, "Novel microwave microfluidic sensor using a microstrip split-ring resonator," *IEEE Transactions on Microwave Theory and Techniques*, vol. 62, no. 3, pp. 679–688, 2014.

[17] A. A. Abduljabar, N. Clark, J. Lees, and A. Porch, "Dual mode microwave microfluidic sensor for temperature variant liquid characterization," *IEEE Transactions on Microwave Theory and Techniques*, vol. 65, no. 7, pp. 2572–2582, 2017.

[18] A. Bhat, P. V. Gwozdz, A. Seshadri, M. Hoeft, and R. H. Blick, "A tank-circuit for ultrafast single particle detection in micropores," *arXiv preprint arXiv:1711.01126*, 2017.

[19] M. Nikolic-Jaric, S. Romanuik, G. Ferrier, G. Bridges, M. Butler, K. Sunley, D. Thomson, and M. Freeman, "Microwave frequency sensor for detection of biological cells in microfluidic channels," *Biomicrofluidics*, vol. 3, no. 3, p. 034103, 2009.

[20] G. Yesiloz, M. S. Boybay, and C. L. Ren, "Label-free high-throughput detection and content sensing of individual droplets in microfluidic systems," *Lab on a Chip*, vol. 15, no. 20, pp. 4008–4019, 2015.

[21] I. Bargatin, E. Myers, J. Arlett, B. Gudlewski, and M. Roukes, "Sensitive detection of nanomechanical motion using piezoresistive signal downmixing," *Applied Physics Letters*, vol. 86, no. 13, p. 133109, 2005.

[22] M. S. Hanay, S. Kelber, A. Naik, D. Chi, S. Hentz, E. Bullard, E. Colinet, L. Duraffourg, and M. Roukes, "Single-protein nanomechanical mass spectrometry in real time," *Nature nanotechnology*, vol. 7, no. 9, p. 602, 2012.

[23] M. S. Hanay, S. I. Kelber, C. D. O'Connell, P. Mulvaney, J. E. Sader, and M. L. Roukes, "Inertial imaging with nanomechanical systems," *Nature nanotechnology*, vol. 10, no. 4, p. 339, 2015.

[24] M. Abdolrazzaghi, M. H. Zarifi, M. Daneshmand, and C. F. Floquet, "Contactless asphaltene solid particle deposition monitoring using active microwave resonators," in *SENSORS, 2016 IEEE*, pp. 1–3, IEEE, 2016.

[25] S. Ingebrandt, "Bioelectronics: sensing beyond the limit," *Nature nanotechnology*, vol. 10, no. 9, p. 734, 2015.

[26] D. M. Pozar, "Microwave engineering 3e," *Tramsmission Lines and Waveguides*, pp. 143–149, 2005.

[27] M. Kelleci, H. Aydogmus, L. Aslanbas, S. O. Erbil, and M. S. Hanay, "Towards microwave imaging of cells," *Lab on a Chip*, vol. 18, no. 3, pp. 463–472, 2018.

[28] Z. Li, R. Zhao, T. Koschny, M. Kafesaki, K. B. Alici, E. Colak, H. Caglayan, E. Ozbay, and C. Soukoulis, "Chiral metamaterials with negative refractive index based on four "u" split ring resonators," *Applied Physics Letters*, vol. 97, no. 8, p. 081901, 2010.

[29] F. Martın, J. Bonache, F. a. Falcone, M. Sorolla, and R. Marqués, "Split ring resonator-based left-handed coplanar waveguide," *Applied Physics Letters*, vol. 83, no. 22, pp. 4652–4654, 2003.

[30] K. Aydin, I. Bulu, K. Guven, and E. Ozbay, "Transmission properties of various split-ring resonator systems," in *Quantum Electronics and Laser Science Conference*, p. JTuD44, Optical Society of America, 2006.

[31] K. B. Alici and E. Ozbay, "Electrically small split ring resonator antennas," *Journal of applied physics*, vol. 101, no. 8, p. 083104, 2007.

[32] I. Bulu, H. Caglayan, K. Aydin, and E. Ozbay, "Compact size highly directive antennas based on the srr metamaterial medium," *New Journal of Physics*, vol. 7, no. 1, p. 223, 2005.

[33] R. Penciu, K. Aydin, M. Kafesaki, T. Koschny, E. Ozbay, E. Economou, and C. Soukoulis, "Multi-gap individual and coupled split-ring resonator structures," *Optics Express*, vol. 16, no. 22, pp. 18131–18144, 2008.

[34] M. M. Radmanesh, *Radio frequency and microwave electronics illustrated*. Prentice Hall New Jersey, 2001.

[35] Z. Instruments, *Principles of lock-in detection and the state of the art*. Zurich Instruments.

[36] P. Lee, "Low noise amplifier selection guide for optimal noise performance," *Analog Devices Application Note, AN-940*, 2009.

[37] J. A. Barnes, A. R. Chi, L. S. Cutler, D. J. Healey, D. B. Leeson, T. E. McGunigal, J. A. Mullen, W. L. Smith, R. L. Sydnor, R. F. Vessot, *et al.*, "Characterization of frequency stability," *IEEE transactions on instrumentation and measurement*, vol. 1001, no. 2, pp. 105–120, 1971.

[38] D. W. Allan, "Should the classical variance be used as a basic measure in standards metrology?," *IEEE Transactions on instrumentation and measurement*, vol. 1001, no. 2, pp. 646–654, 1987.

[39] D. W. Allan, "Statistics of atomic frequency standards," *Proceedings of the IEEE*, vol. 54, no. 2, pp. 221–230, 1966.

[40] K. Chang and L.-H. Hsieh, *Microwave ring circuits and related structures*, vol. 156. John Wiley & Sons, 2004.

[41] T. S. Laverghetta, *Microwave materials and fabrication techniques*. Artech House, 2000.

[42] L. K. Baxter, "Capacitive sensors," *Ann Arbor*, vol. 1001, p. 48109, 2000.

Appendix A

Derivation

Taking the derivative of the expression in the RHS of 1.10:

$$\frac{d}{d\alpha_i^k}\int(\Sigma_n^N|\Phi_n(x)|^2)^2dx-2\frac{d}{d\alpha_i^k}\int\Sigma_n^N|\Phi_n(x)|^2g_{exact}(x)dx+\frac{d}{d\alpha_i^k}\int g_{exact}^2(x)dx=0 \tag{A.1}$$

The third term on the left-hand side vanishes since it does not contain the α term. At this step define the first term in A.1 as Γ_1 and the second one as Γ_2. After applying the square, Γ_1 becomes:

$$\Gamma_1=\frac{d}{d\alpha_i^k}\int\Sigma_n^N\Sigma_m^N\alpha_n^k\alpha_m^k|\Phi_n(x)|^2|\Phi_m(x)|^2dx \tag{A.2}$$

Define the dirac-delta function for the derivative operation as $\frac{d\alpha_j}{d\alpha_i^k}=\delta_{ij}$. Henceforth, Γ_1 after application of derivative becomes:

$$\Gamma_1=\int\Sigma_n^N\Sigma_m^N(\alpha_n^k\delta_{im}+\alpha_m^k\delta_{in})|\Phi_n(x)|^2|\Phi_m(x)|^2dx \tag{A.3}$$

Therefore:

$$\Gamma_1 = \int \Sigma_n^N |\Phi_n(x)|^2 |\Phi_m(x)|^2 dx + \int \Sigma_m^N |\Phi_n(x)|^2 |\Phi_m(x)|^2 dx \tag{A.4}$$

Since the series run within the same interval, Γ_1 can be further simplified to as follows:

$$\Gamma_1 = 2\Sigma_n^N \alpha_n^k \int |\Phi_n(x)|^2 |\Phi_m(x)|^2 dx \tag{A.5}$$

As for the term Γ_2 the derivative applies as follows:

$$\Gamma_2 = -2\delta_{in} \int g_{exact}(x) |\Phi_n(x)|^2 dx \tag{A.6}$$

Therefore equation for $\frac{de}{d_{\alpha_n^k}}$ can be written as follows:

$$\Sigma_n^N \int |\Phi_n(x)|^2 |\Phi_m(x)|^2 dx = \int g_{exact}(x) |\Phi_n(x)|^2 dx \tag{A.7}$$

Since the expression contains multiple number of equations, after defining the term on the LHS as the product of $T_{mn}\alpha_n^k$ and the term on the RHS as b_m the expression becomes a linear system of equations as follows:

$$T_{mn}\alpha_n^k = b_m \tag{A.8}$$

In conclusion, if the function T_{mn}^{-1} exist so that there exist a unique solution, the weighing coefficients can be determined as follows.

$$\alpha_n^k = b_m T_{mn}^{-1} \tag{A.9}$$